

**DEEP LEARNING ANALYSIS IN DERMOSCOPY IMAGES  
(DERMOSKOPİ GÖRÜNTÜLERİİNDE DERİN ÖĞRENME ANALİZİ)**

by

**FATİH ERGİN, B.S.**

**Thesis**

Submitted in Partial Fulfillment

of the Requirements

for the Degree of

**MASTER OF SCIENCE**

in

**COMPUTER ENGINEERING**

in the

**GRADUATE SCHOOL OF SCIENCE AND ENGINEERING**

of

**GALATASARAY UNIVERSITY**

**JULY 2020**

Approval of the thesis:

## DEEP LEARNING ANALYSIS IN DERMOSCOPY IMAGES

submitted by **FATİH ERGİN** in partial fulfillment of the requirements for the degree of **Master of Science** in **Computer Engineering Department, Galatasaray University** by,

### Examining Committee Members:

Assist. Prof. Dr. İ. BURAK PARLAK  
Supervisor, **Computer Engineering Department, GSU**

Prof. Dr. TANKUT ACARMAN  
**Computer Engineering Department, GSU**

Prof. Dr. RESUL DAŞ  
**Software Engineering Department, Fırat University**

Date:

## **ACKNOWLEDGMENTS**

I would like to express my sincere gratitude to my supervisor Assist. Prof. Dr. İ. Burak Parlak for supporting and guiding me, sharing his knowledge, helping me learn and grow and become a better researcher over the duration of my Masters program.

I would also thank my family and my friends for their motivating and supporting attitudes.

## TABLE OF CONTENTS

ACKNOWLEDGEMENTS . . . . .	iii
TABLE OF CONTENTS . . . . .	iv
LIST OF FIGURES . . . . .	vi
LIST OF TABLES . . . . .	ix
ABSTRACT . . . . .	x
RÉSUMÉ . . . . .	xii
ÖZET . . . . .	xiv
LIST OF ABBREVIATIONS . . . . .	xvi
1 INTRODUCTION . . . . .	1
2 RELATED WORKS . . . . .	4
2.1 Medical Imaging Techniques . . . . .	4
2.1.1 Common Diagnostic Modalities . . . . .	4
2.1.2 Dermatology Imaging Techniques . . . . .	7
2.2 Image Segmentation Architectures . . . . .	8
2.2.1 Fully Convolutional Network . . . . .	8
2.2.2 SegNet . . . . .	9
2.2.3 U-Net . . . . .	9
2.2.4 Generative Adversarial Network . . . . .	11
2.3 Related Works . . . . .	11
3 NEURAL NETWORKS IN TUMOR DETECTION . . . . .	19
3.1 Artificial Neural Networks . . . . .	19
3.1.1 Weight Update . . . . .	20
3.1.2 Activation Functions . . . . .	20

3.1.3	Loss Functions . . . . .	23
3.2	Convolutional Neural Networks . . . . .	24
3.3	Regularization Techniques . . . . .	25
4	METHODOLOGY . . . . .	28
4.1	Dataset . . . . .	28
4.2	Networks . . . . .	30
4.2.1	MultiResUNet . . . . .	30
4.2.2	SegAN . . . . .	32
4.3	Tools and Frameworks . . . . .	33
4.4	Experiments . . . . .	35
4.5	Evaluation Metrics . . . . .	36
5	RESULTS . . . . .	38
6	DISCUSSION . . . . .	45
7	CONCLUSION . . . . .	46
	REFERENCES . . . . .	47
	BIOGRAPHICAL SKETCH . . . . .	54

## LIST OF FIGURES

Figure 1.1 Flowchart of the analysis . . . . .	3
Figure 2.1 Medical Imaging Concept . . . . .	4
Figure 2.2 Sample X-ray Images . . . . .	5
Figure 2.3 Sample MRI Images (Lövblad et al., 2010) . . . . .	5
Figure 2.4 Sample CT Images (Chilamkurthy et al., 2018) . . . . .	6
Figure 2.5 Sample Multispectral Images (Dhawan et al., 2009) . . . . .	7
Figure 2.6 From right to left clinical, dermoscopical, confocal images of a skin lesion (Ruini et al., 2016) . . . . .	8
Figure 2.7 SegNet architecture (Badrinarayanan et al., 2017) . . . . .	9
Figure 2.8 U-Net architecture (Ronneberger et al., 2015) . . . . .	10
Figure 2.9 GAN architecture . . . . .	11
Figure 3.1 A sample ANN model . . . . .	19
Figure 3.2 Nonlinear activation functions <b>(a)</b> Sigmoid, <b>(b)</b> Tanh, <b>(c)</b> ReLU, and <b>(d)</b> Leaky ReLU (Yang and Yang, 2018) . . . . .	21
Figure 3.3 A CNN architecture for skin lesion classification . . . . .	24
Figure 3.4 Dropout neural network model . . . . .	26
Figure 4.1 Sample skin lesions from the dataset. . . . .	29

Figure 4.2 Data preparation process . . . . .	29
Figure 4.3 Evalution of MultiRes block : <b>(a)</b> Inception-like block <b>(b)</b> a more expensive attempt <b>(c)</b> MultiRes block (Ibtehaz and Rahman, 2020) . . . . .	30
Figure 4.4 Proposed Res path with residual connections (Ibtehaz and Rahman, 2020) . . . . .	31
Figure 4.5 MultiResUnet architecture . . . . .	31
Figure 4.6 SegAN architecture . . . . .	33
Figure 5.1 SegAN result with average score at 0% of Gaussian noise . . . . .	38
Figure 5.2 SegAN result with low success compared to average at 0% of Gaussian noise . . . . .	39
Figure 5.3 SegAN result with high success compared to average at 0% of Gaussian noise . . . . .	39
Figure 5.4 MultiResUNet result with average score at 0% of Gaussian noise . .	39
Figure 5.5 MultiResUNet result with low success compared to average at 0% of Gaussian noise . . . . .	40
Figure 5.6 MultiResUNet result with high success compared to average at 0% of Gaussian noise . . . . .	40
Figure 5.7 Dice results for U-Net at different Gaussian noises by number of epochs	41
Figure 5.8 Dice results for SegAN at different Gaussian noises by number of epochs	41
Figure 5.9 Dice results for MultiResUNet at different Gaussian noises by number of epochs . . . . .	42
Figure 5.10Comparision of the results of the models at different noise levels . .	42
Figure 5.11Change of success of the models by noise level . . . . .	42

Figure 5.12 Dice results of the same image for the all networks at different Gaussian noises. The images in a column from top to bottom show the input, results of MultiResUnet, SegAN, and U-Net respectively. SegAN has better results . . . . . 43

Figure 5.13 Dice results of the same image for the all networks at different Gaussian noises. The images in a column from top to bottom show the input, results of MultiResUnet, SegAN, and U-Net respectively. U-Net has better results . . . . . 43

## LIST OF TABLES

Table 2.1 Comparision of medical imaging techniques . . . . .	6
Table 2.2 Summary of related skin lesion segmentation surveys . . . . .	15
Table 5.1 Comparision of segmentation results of U-Net at different levels of Gaussian noise with evaluation metrics . . . . .	44
Table 5.2 Comparision of segmentation results of SegAN at different levels of Gaussian noise with evaluation metrics . . . . .	44
Table 5.3 Comparision of segmentation results of MultiResUNet at different levels of Gaussian noise with evaluation metrics . . . . .	44

## ABSTRACT

Computer assisted radiology becomes an interdisciplinary domain between mathematics, medicine and engineering. Tumor detection, analysis, classification are main problems in digital radiology for diagnosis and follow-up. A physician or an oncologist involves in the care of patients by regarding detailed reports of carcinoma in situ that analyze the pathology of suspicious lesions. Deep learning applied to several fields in medicine is considered as an intervention for oncology. Even if the final treatment of the lesion is decided by the oncologists or the surgeons in a case of resection, image based analysis of lesions (benign or malign) promises automated decision making for radiology. Because of the increased ability of machine learning techniques to transform input data into high level presentations, deep learning techniques used for image analysis have become important for helping physicians in the last few years. Skin lesion detection and classification are current challenges in medical image analysis. Skin diseases are difficult to recognize because of the similarity between lesions and low contrast between the lesions and the skin. Dermatologic image processing benefits from the evaluation scores of neural nets. To help the physicians for the accurate diagnosis, the medical field has an increasing interest in this technology, especially in the diagnosis of skin lesions. This thesis presents a comparision between various state-of-the-art deep learning frameworks namely U-Net, SegAN and MultiResUNet to solve skin lesion analysis problems using a dermatoscopic image that contains a skin tumor. SegAN which is a special type of Generative Adversarial Network (GAN) brings a new architecture in machine learning by adding generator and discriminator steps in data analysis. MultiResUNet is a U-Net-based neural network architecture which aims to overcome the insufficient data problem in medical imaging field by extracting contextual details even if the dataset is small. In this thesis, U-Net, SegAN and MultiResUNet architectures have been implemented on two dimensional skin lesion images from the International Symposium on Biomedical Imaging (ISBI) 2017 Challenge. After the preprocessing, colored images have been trained in U-Net, SegAN and MultiResUNet. The experiment setup has been enriched by adding incremental noise on tumor images before models training. The evaluation has been tested through accuracy, sensitiv-

ity, specificity, Dice coefficient and Jaccard coefficient parameters. In conclusion, test results showed that both SegAN and MultiResUNet architectures provide a robust approach against U-Net which is well known medical image segmentation framework in skin lesion analysis.

**Keywords :** DEEP LEARNING, IMAGE PROCESSING, MEDICAL IMAGING, MACHINE LEARNING, NEURAL NETWORKS

## RÉSUMÉ

La radiologie assistée par ordinateur devient un domaine interdisciplinaire entre les mathématiques, la médecine et l'ingénierie. La détection, l'analyse, la classification des tumeurs sont les principaux problèmes en radiologie numérique pour le diagnostic et le suivi. Un médecin ou un oncologue intervient dans la prise en charge des patients en consultant des rapports détaillés de carcinome *in situ* qui analysent la pathologie des lésions suspectes. L'apprentissage profond appliqué à plusieurs domaines de la médecine est considéré comme une intervention en oncologie. Même si le traitement final de la lésion est décidé par les oncologues ou les chirurgiens en cas de résection, l'analyse d'images des lésions (bénignes ou malignes) promet une prise de décision automatisée en radiologie. En raison de la capacité accrue des techniques d'apprentissage automatique à transformer les données d'entrée en présentations de haut niveau, les techniques d'apprentissage approfondi utilisées pour l'analyse d'images sont devenues importantes pour aider les médecins au cours des dernières années. La détection et la classification des lésions cutanées sont des défis actuels dans l'analyse d'images médicales. Les maladies de la peau sont difficiles à reconnaître en raison de la similitude entre les lésions et du faible contraste entre les lésions et la peau. Le traitement d'image dermatologique bénéficie des scores d'évaluation des réseaux neuronaux. Pour aider les médecins à poser un diagnostic précis, le domaine médical s'intéresse de plus en plus à cette technologie, notamment au diagnostic des lésions cutanées. Cette thèse présente une comparaison entre divers cadres d'apprentissage en profondeur de pointe, à savoir U-Net, SegAN et MultiResUNet pour résoudre les problèmes d'analyse des lésions cutanées à l'aide d'une image dermatoscopique contenant une tumeur cutanée. SegAN qui est un type spécial de Réseau Génératif Adversaire (GAN) apporte une nouvelle architecture dans l'apprentissage automatique en ajoutant des étapes de générateur et de discriminateur dans l'analyse des données. MultiResUNet est une architecture de réseau neuronal basée sur U-Net qui vise à surmonter le problème de données insuffisantes dans le domaine de l'imagerie médicale en extrayant des détails contextuels même si l'ensemble de données est petit. Dans cette thèse, les architectures U-Net, SegAN et MultiResUNet ont été implémentées sur des images de lésions cutanées bidimensionnelles Défi 2017

du Symposium international sur l'imagerie biomédicale (ISBI). Après le prétraitement, des images en couleur ont été formées en U-Net, SegAN et MultiResUNet. La configuration de l'expérience a été enrichie par l'ajout de bruit incrémentiel sur les images tumorales avant la formation des modèles. L'évaluation a été testée par les paramètres d'exactitude, de sensibilité, de spécificité, de coefficient de dés et de coefficient de Jaccard. En conclusion, les résultats des tests ont montré que les architectures SegAN et MultiResUNet fournissent une approche robuste contre U-Net qui est un cadre de segmentation d'image médicale bien connu dans l'analyse des lésions cutanées.

**Mots Clés :** L'APPRENTISSAGE EN PROFONDEUR, TRAITEMENT D'IMAGE, L'IMAGERIE MÉDICALE, APPRENTISSAGE DE LA MACHINE, LES RÉSEAUX DE NEURONES

## ÖZET

Bilgisayar destekli radyoloji, matematik, tip ve mühendislik arasında disiplinlerarası bir alan haline gelmiştir. Tümör tespiti, analizi ve sınıflandırması, tanı ve takip için dijital radyolojideki temel problemlerdendir. Bir doktor veya onkolog, şüpheli lezyonların patolojisini analiz eden in situ karsinomun detaylı raporlarını dikkate alarak hastaların bakımında yer alır. Tıpta çeşitli alanlara uygulanan derin öğrenme, onkolojiye bir müdahale olarak kabul edilir. Rezeksiyon durumunda lezyonun son tedavisine onkologlar veya cerrahlar karar verse bile, görüntü temelli lezyon (iyi huylu veya kötü huylu) analizi, radyolojide otomatik karar vermeyi vaat eder. Son yıllarda makine öğrenimi tekniklerinin insan algısı için anlamsız olabilecek verileri anlamlı hale dönüştürme yeteneğinin artmasıyla beraber, görüntü analizi için kullanılan derin öğrenme teknikleri, son yıllarda hekimlere yardımcı olan önemli bir araç haline gelmiştir. Deri lezyonlarının saptanması ve sınıflandırılması tıbbi görüntü analizinde güncel zorluklardandır. Lezyonlar arasındaki benzerlik ve lezyonlar ile cilt arasındaki düşük kontrast nedeniyle cilt hastalıklarını tanımak zordur. Dermatolojik görüntü işleme, doktorların doğru tanı koymasına yardımcı olmak için bu teknolojiyle, özellikle cilt lezyonlarının teşhisile ilgili olan kısmına yoğun ilgi göstermektedir. Bu tez, U-Net, bir generatif adversial ağ (GAN) türevi olan SegAN ve MultiResUNet gibi son teknoloji derin öğrenme yaklaşımlarıyla cilt tümörü içeren dermatoskopik görüntüleri kullanarak cilt lezyonu analiz problemlerini çözmeye yol göstermeyi amaçlayan bir çalışma sunmaktadır. SegAN, klasik CNN'lerden farklı olarak derin öğrenme modeline üretici ve ayırıcı adımlar ekleyerek yeni bir mimari sunmuştur. MultiResUNet, medikal görüntüleme alanının temel sorunlarından biri olan yetersiz veri problemini bağlamsal detayları az veriden başarılı bir şekilde çıkararak aşmayı amaçlayan bir derin sinir ağı mimarisidir. Bu makalede, U-Net, SegAN ve MultiResUNet mimarileri Uluslararası Biyomedikal Görüntüleme Sempozyumu (ISBI) 2017 Yarışması'ndan alınan iki boyutlu cilt lezyonu görüntüleri üzerine uygulanmıştır. Ön işlemeden sonra, renkli görüntüler hem SegAN da hem de MultiResUNet'te eğitilmiştir. Deney düzeneği, model eğitimi öncesinde tümör görüntülerine artımlı gürültü eklenerek zenginleştirilmiştir. Değerlendirme; doğruluk, duyarlılık, özgüllük, Dice katsayısı ve Jaccard katsayısı parametreleri ile yapılmıştır. Sonuç olarak,

test sonuçları hem SegAN hem de MultiResUNet mimarilerinin cilt lezyonu analizinde, farklı gürültü oranlarında tutarlı bir yaklaşım sağladığını ve U-Net mimarisine göre daha başarılı olduklarını göstermiştir.

**Anahtar Kelimeler :** DERİN ÖĞRENME, GÖRÜNTÜ İŞLEME, MEDİKAL GÖRÜNTÜLEME, MAKİNE ÖĞRENMESİ, SİNİR AĞLARI

## LIST OF ABBREVIATIONS

ANN	Artificial Neural Network
BCE	Balanced Cross Entropy
BGD	Batch gradient descent
CDNN	Convolutional Deconvolutional Neural Network
CLSM	Confocal Laser Scanning Microscopy
CNN	Convolutional Neural Network
CT	Computed Tomography
DDN	Dense Deconvolutional Network
DIT	Dermoscopy Imaging Technique
DNN	Deep Neural Network
FCN	Fully Convolutional Network
FCRN	Fully Convolutional Residual Network
GAN	Generative Adversarial Network
ISBI	International Symposium on Biomedical Imaging
ISIC	International Skin Imaging Collaboration
MI	Multispectral Imaging
MIT	Medical Imaging Techniques
MRI	Magnetic Resonance Imaging
PIL	Python Imaging Library
ReLU	Rectified Linear Unit
SGD	Stochastic gradient descent
TP	Traditional Photography
WCE	Weighted Cross Entropy

## 1 INTRODUCTION

During the last few years, deep neural networks have gained considerable attention in several problems of computer vision. The new network hierarchies present complex transfer modalities to deal with adaptive learning tasks. Deep neural networks (DNN) allow machines to learn hybrid data structures of mathematical models which can be used to achieve comprehensive data analysis. Image semantics would be resolved using relevant models. The learning rate is measured in DNN by the achievement of comprehensive data analysis. Generative adversarial networks (GANs) deal with a new hierarchy in intelligent systems. The network scheme conforms to better training performance with less annotations. GAN achievement is derived through a competitive learning where the model consists of different stacks. The processing in layers is characterized with multiple levels of abstraction from high-dimensional input data.

In medicine, lesion detection becomes more efficient with new models based on deep learning networks from histological to radiological acquisitions. Recent studies reveal that detection performance of deep networks has even matched or exceeded human-level performance in several tasks such as diabetic retinopathy and tumor detection (Gulshan et al., 2016),(Işın et al., 2016). Early detection of cancer is considered as one the most complex and hard problems in radiology. The follow-ups and repeated cases are also challenges for the correct decision making. Over the last decade, the progress and the integration of DNN enable rapid diagnosis of patients at these risk groups. Even if the final medical decision must be taken with a specialist, DNNs might reduce the time for the diagnostic errors and workload of physicians. Therefore, DNN performance is not compared with physicians in our study. The evaluation of DNN based segmentation is performed through Ground Truth ; a mask which identifies the whole area or volume in target images.

The common goal of deep learning techniques is to recursively learn computational model parameters using a training dataset to gradually improve the model in performing the desired purpose. Using many previously unseen data, models can also perform the same task accurately once a computer is trained for a specific task. Deep learning is distinguish from the other techniques of machine learning because of its strong generalization ability. The detection and evaluation criteria result that the use of multilayered hierarchy of GAN shows valid scores. The variation of inter observer, the inhomogeneity in image scale encompass the complexity of automatic lesion detection. In skin lesion

segmentation, International Skin Imaging Collaboration (ISIC) focuses on the analysis and the improvement of big datasets. Annotated image corpora is considered as a challenge in deep learning for detection and classification. Even if recent studies in data challenges promised valid results for clinical applications, the performance evaluation shows that training datasets might cause variation in skin lesion detection. In order to promote automatic analysis in this field, GAN technique that represents promising scores is preferred. Although many studies have been presented in this area, it can be seen that the success in the field of skin segmentation can be increased even further. The International Skin Imaging Collaboration (ISIC) focused on automatic analysis of skin lesions, it has been trying to enrich the dataset regularly since 2016. Annotated skin lesion images are presented by ISIC for ISBI 2017 Challenge which can be used in feature extraction for automatic lesion segmentation tasks.

In this thesis, we provide a new application area of deep neural networks in skin lesion analysis. We note that dermoscopic feature extraction is relatively a new problem in deep learning to address the detection and the classification of lesions. The following section presents the medical imaging techniques, image segmentation architectures for automatic diagnosis of skin lesions from dermoscopic images and related studies of DNN for medicine. The third section shows the basis of neural networks and convolutional neural networks. Used neural network architectures, dataset, tools and deep learning frameworks are explained in fourth section along with our corresponding formulation through computational parameters and the statistical evaluation. Our detection results are given through statistical parameters in the fifth section. Finally, the assessment of examined neural networks in skin lesion detection is concluded through the current state-of-the-art and prospective improvements. The flow of the study in this thesis is summarized in Figure 1.1.

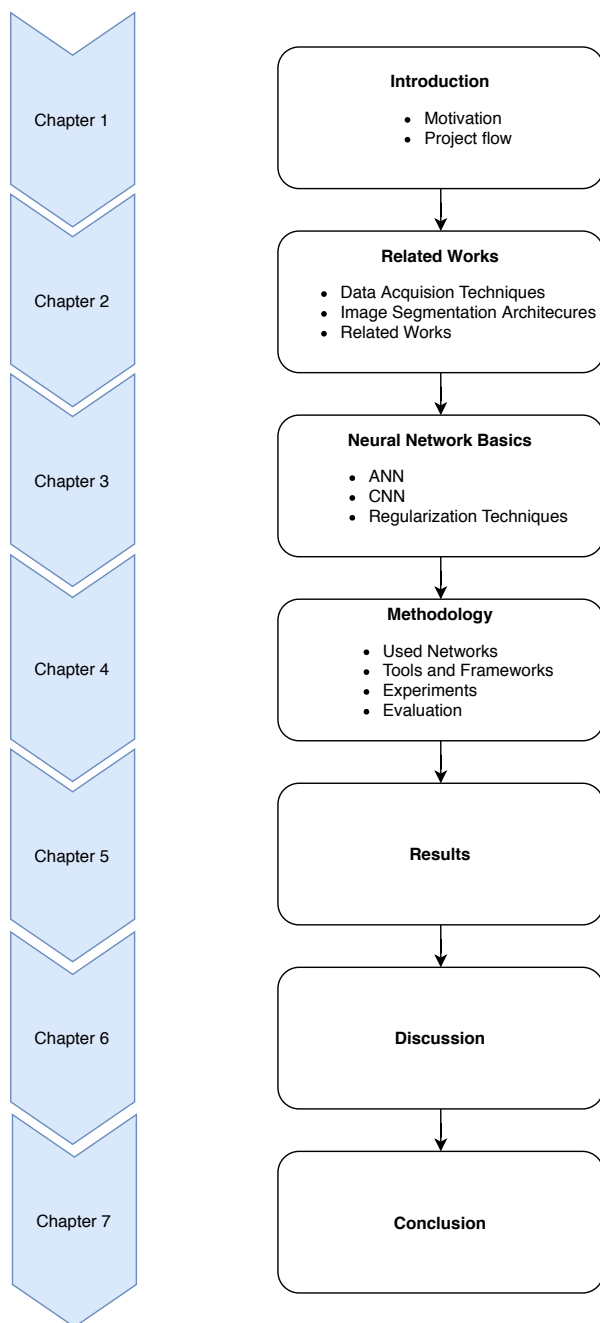


Figure 1.1: Flowchart of the analysis

## 2 RELATED WORKS

In this section, both common medical imaging techniques and dermatology imaging techniques are presented. Furthermore, skin lesion segmentation is detailed through commonly image segmentation architectures. Finally, related works are given to illustrate recent approaches in dermoscopic image analysis

### 2.1 Medical Imaging Techniques

Medical Image Segmentation aims to determine the location and shape of the body part or structure within a 2D or 3D image automatically or semi-automatically (Merjulah and Chandra, 2019). The medical images are acquired using different modalities. Wide modality range and the high variability of human anatomy is the major difference of medical image segmentation. Medical images are divided into several interests related with the problem definition to detect or segment the tumor or mass. Irregularities, blurred vision borders, low contrast between lesion and skin, air bubbles are the some of various artifacts that makes segmentation medical imaging challenging (Guo and Ashour, 2019).

Medical Imaging Techniques (MIT) are concerned to create medical images to be able to examine internal structures of body without opening up it (Kasban et al., 2015). In this section, common medical imaging techniques are being investigated.

#### 2.1.1 Common Diagnostic Modalities

This section represent the review of widely-used medical imaging techniques namely X-ray Radiography, Magnetic Resonance Imaging, and Computed Tomography. The flowchart of a generic procedure in medical imaging is given in Figure 2.1.

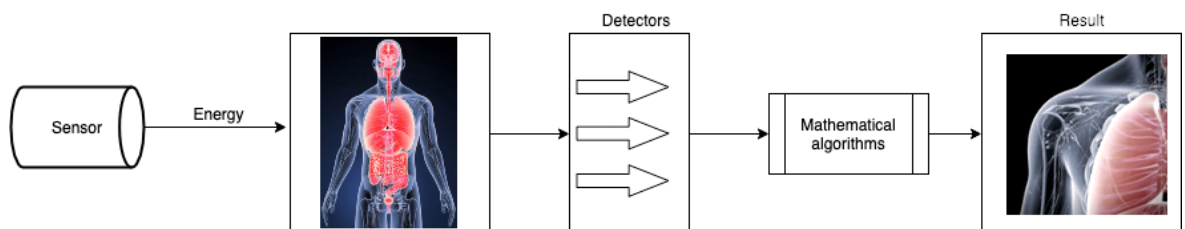


Figure 2.1: Medical Imaging Concept



Figure 2.2: Sample X-ray Images

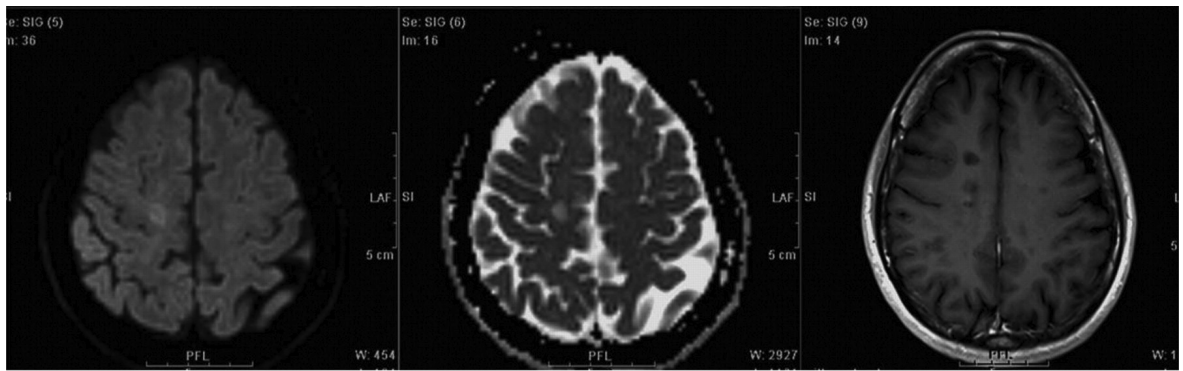


Figure 2.3: Sample MRI Images (Lövblad et al., 2010)

- **X-ray Radiography** is an imaging technique that uses ionizing electromagnet radiation, such as X-ray which is a type of high-energy electromagnetic radiation (Kasban et al., 2015). As it can be seen in Figure 2.2, there is a trade-off between radiation level and image contrast which should be chosen carefully. X-ray passes through the body and is absorbed at different levels according to several factors such as the different tissue density. Mammography which deals with the scanning of breast tissue is one of the well-known application areas of X-ray Radiography.
  - **Magnetic Resonance Imaging (MRI)** is a commonly used imaging techniques for medical tasks which uses magnetic fields and frequencies in the radio wave spectrum to create images of body tissue (Mehmood et al., 2013). Magnetic spin relaxation times and proton density changes can be used as distinctive in detecting abnormal tissues. MRI is based on visualizing these changes. MRI imaging can be enhanced by using a contrast solution, e.g. gadolinium, which will change the relaxation properties of some tissues under certain conditions.
- Advantages of using MRI include painless, ionizing-free radiation, and high spatial resolution with operator independent usage. MRI does not offer real time results because of the relatively long scanning and post processing time. Moreo-

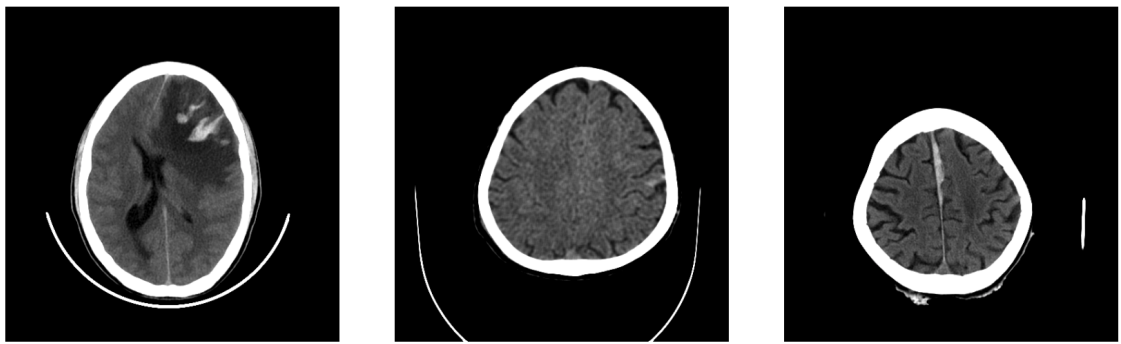


Figure 2.4: Sample CT Images (Chilamkurthy et al., 2018)

ver, patient comfort is an issue due to limited space within the gantry and long acquisition time. An MRI sample is shown in Figure 2.3.

- **Computed Tomography (CT)** is supported with a cathode ray tube used to create detailed image of parts of the human body such as internal organs, blood vessels, bones and soft tissues. CT scanning is a common method in cancer diagnosis, as it is widely used to determine the size and location of a tumor. It is used to create not only for two dimensional (2D) images but also for three dimensional (3D) images using spiral CT which is basically reconstructing the collected volume data to provide 3D images. Figure 2.4 shows some examples of generated CT images.

Analyzing the parts of human body, diagnosing the abnormalities and traumas, observing the results of the cancer treatments are the common use cases of CTs. It comes with several benefits such as getting good spatial resolution, detecting issues quickly and painlessly. On the other hand, CTs do not provide real time analysis and relatively useless results with the soft tissues with low contrast.

Table 2.1: Comparision of medical imaging techniques

Imaging Techniques	Spatial resolution	Good contrast	Cost	Real time visualization
Ultrasonography	1mm	Soft tissues	Low	Supported
X-ray	1mm	Soft tissues and fluid	Medium	Unsupported
CT	0.5mm	Hard and soft tissues	High	Unsupported
MRI	0.5mm	Hard and soft tissues	High	Unsupported

A general comparison for common medical imaging technique is given in Table 2.1. Ultrasonography which is the first technique in Table 2.1 is examined in Section

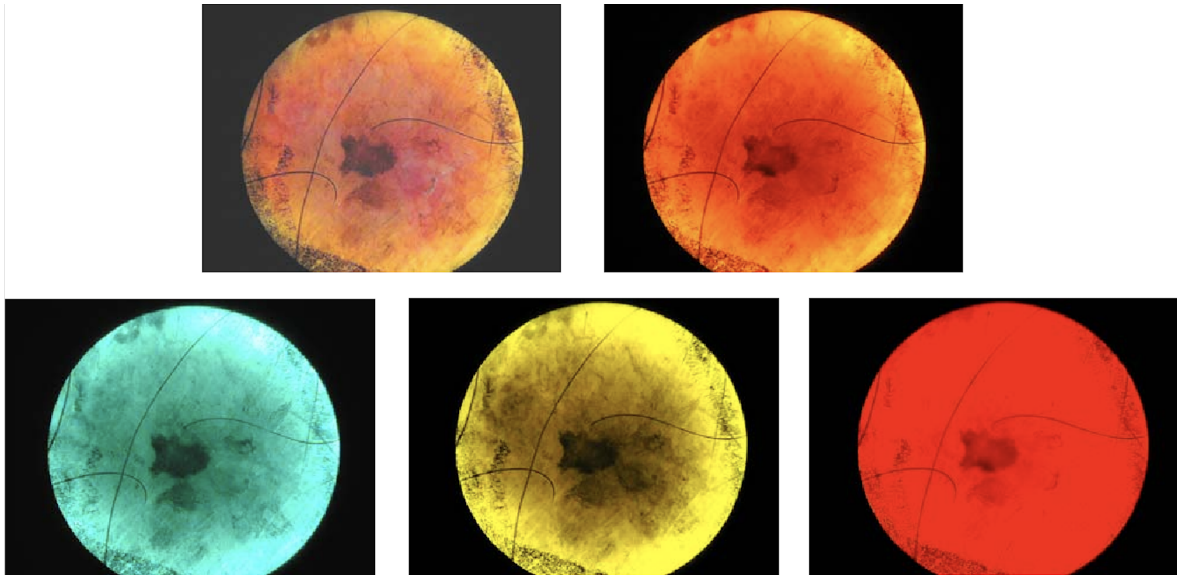


Figure 2.5: Sample Multispectral Images (Dhawan et al., 2009)

### 2.1.2.

#### 2.1.2 Dermatology Imaging Techniques

In this section, imaging techniques used in skin lesions are being investigated.

- **Traditional Photography (TP)** is the well-known techniques which makes visualizing and monitoring the top layer of the lesion possible (Feit et al., 2004).
- **Dermoscopy Imaging Technique (DIT)** is a real-time noninvasive diagnostic imaging technique which is more successful in distinguishing melanoma concentration than traditional photography (Aljanabi et al., 2019).
- **Multispectral Imaging (MI)** provides information in both spectral and spatial domains. MI systems increase accuracy by calibrating image intensity, controlling exposure time automatically with the help of a multispectral camera that includes different optical filters selected by the problem definition. MI is used in medical imaging to support detecting the lesions about 2 mm (Aljanabi et al., 2019). Figure 2.5 shows the images of a skin lesion taken by using different optical filters.
- **Confocal Laser Scanning Microscopy (CLSM)** is an imaging technique that provides real-time details of skin morphology and provides images with the same resolution as traditional microscopes (Gerger et al., 2005). CLSMs are very sensitive for clinical applications but they are relatively expensive to use in there.



Figure 2.6: From right to left clinical, dermoscopical, confocal images of a skin lesion (Ruini et al., 2016)

From right to left clinical, dermoscopical, confocal images of a skin lesion is shown in Figure 2.6.

— **Ultrasonography** which is also known as diagnostic sonography is another imaging technique that is used to create medical imaging to create internal body parts using high frequency broadband sound waves. Because different tissues behave differently under these sound waves, the images generated using the waves reflected by tissue (Sahuquillo et al., 2013). Calculating the depth of skin cancer is the focused usage of Ultrasonography for this kind of projects.

Ultrasonography offer painless real time visualization without ionized radiation in high resolution. But it is a time consuming and operator dependent imaging technique.

## 2.2 Image Segmentation Architectures

Fully convolutional network (FCN) is a CNN variant which is a turning point for semantic segmentation literature (Long et al., 2015). After that, many variants of CNN for segmentation have been developed. In this section, commonly used CNNs which are used for image segmentation starting from FCN are examined.

### 2.2.1 Fully Convolutional Network

Fully convolutional networks (FCNs) indicate that the convolutional neural networks are obtained by dismantling the fully connected layers from deep CNNs (Ulku and Akagunduz, 2019). FCNs are built on traditional classification networks such as VGG

(Simonyan and Zisserman, 2014), AlexNet (Krizhevsky et al., 2012), GoogLeNet (Szegedy et al., 2014), and ResNet (He et al., 2016).

Convolutional layers are used instead of fully connected layers to produce outputs with the same size of inputs instead of classification scores which are the outputs of CNNs. FCNs consist of two units encoding and decoding. Convolution and subsampling operations are performed in the encoding unit to encode the lower dimensional latent space. Deconvolution and upsampling are performed in the decoding unit which guarantee the same size of output with the input. Since FCNs do not include fully connected layers, it is faster to get an image with respect to the classical CNNs.

Besides the including convolutional layers, skip architecture is one of the main reasons that makes FCNs faster over CNNs. Skip architectures help to prevent losing some information which can be lost because skip connections are also part of the dropout or any other architectural decisions which may cause losing information. They provide flowing the summed or concatenated data between downsampling and upsampling blocks. Skip connections preserve the localised information which might be lost in pooling layers with bypassing them.

### 2.2.2 SegNet

Badrinarayanan et al. (2017) proposed a FCN based network architecture, called SegNet, aiming to increase the accuracy of segmentation tasks. As it can be seen in Figure 2.7, the encoder network consists of 13 convolutional layers of VGG16 network instead of the original fully connected layers of FCN. A pixel-wise classification layer is added to help the upsampling on the lower resolution images in the decoder network. The upsampling part is the novel improvement of SegNet. Encoder is not fully connected in Segnet. Then, it causes the train parameters to decrease by 90%. There is a corresponding decoder for every 13 encoders and they are responsible for the upsampling of the feature map.

### 2.2.3 U-Net

Ronneberger et al. (2015) proposed a new CNN namely U-Net designed for medical imaging. Because medical image segmentation suffers from lack of large dataset, it is

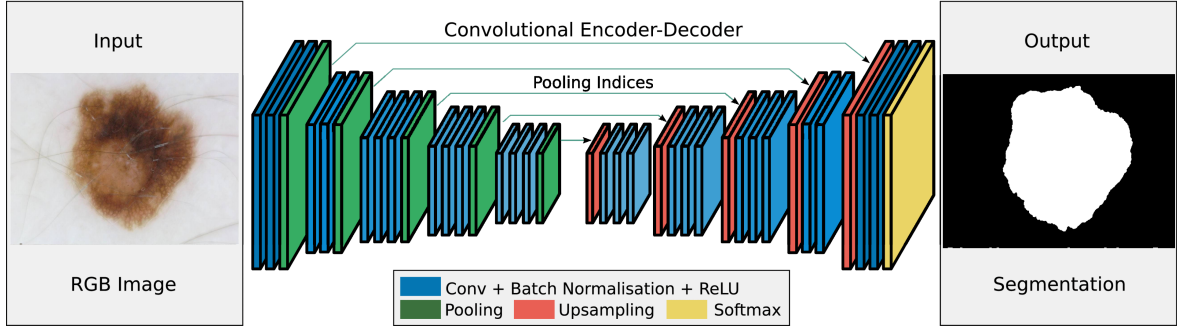


Figure 2.7: SegNet architecture (Badrinarayanan et al., 2017)

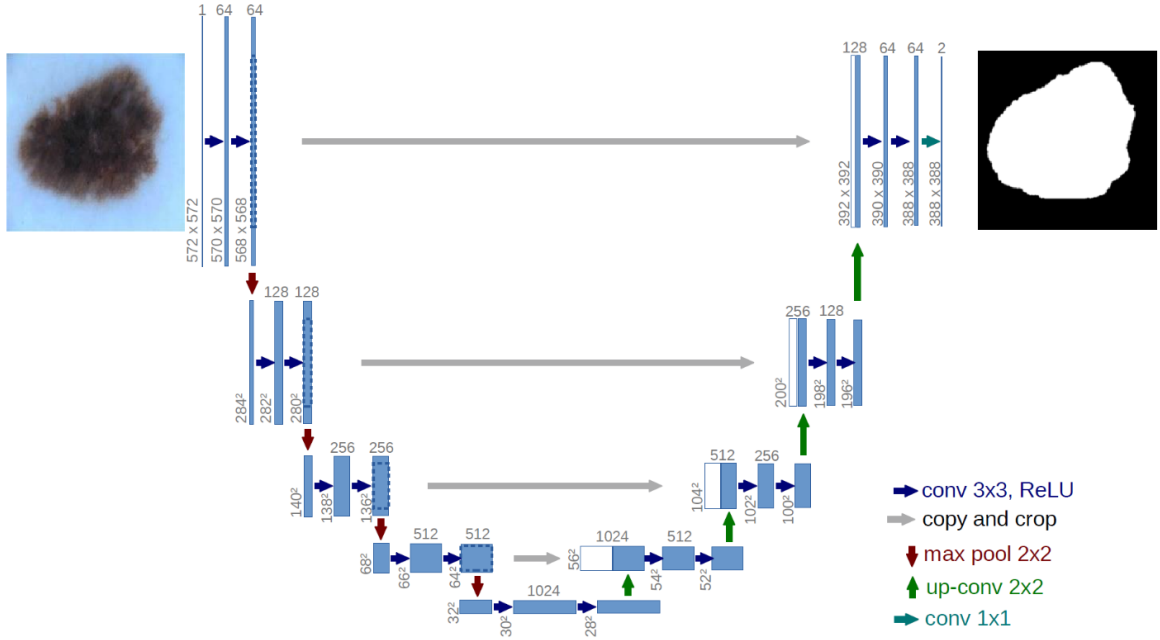


Figure 2.8: U-Net architecture (Ronneberger et al., 2015)

relatively hard to capture image context with localized lesions. U-Net aims to achieve competitive results even if the training data are relatively small.

Classical feed-forward CNNs can learn many small information via the fully connected layers. Large datasets provide a number of parameters to train. However, they are often hard to gather or not accessible in medical domain. U-Net architecture provides more accurate results with smaller datasets by capturing the detailed context. As it can be shown in Figure 2.8, U-Nets are made up of a compact hierarchy using upsampled and downsampled layers till the output layer. These layers are called as contracting and expanding layers respectively in Figure 2.8.

The purpose of the contracting path is to increase resolutions and learn features to capture context while the role of the expanding path is to aid in precise localization with a series of upsampling operations. The contracting path consists of two three-by-

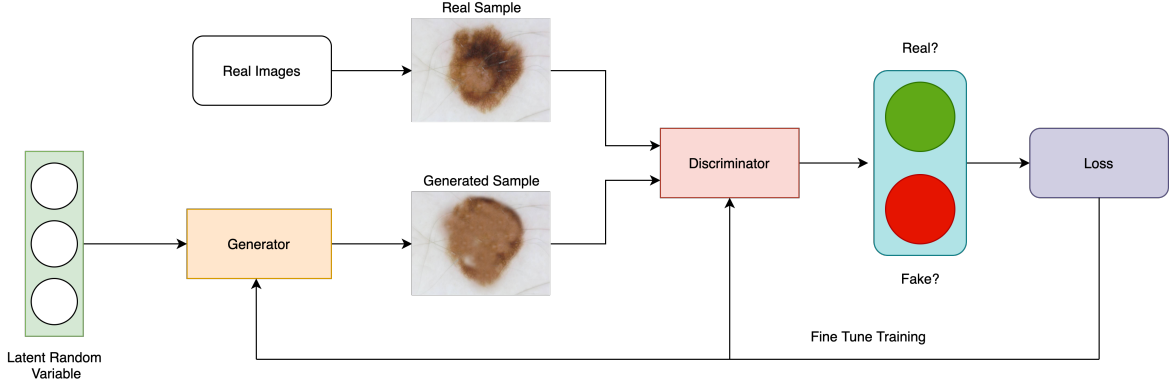


Figure 2.9: GAN architecture

three convolutions followed by a ReLU and two-by-two max pooling layers. On the other side, up convolution layers exist to upsample the outputs. Skip connections help to prevent to lose the spatial context combining with upsampled outputs by transferring the low resolution features to expanding path. The authors used a large-weighted loss function to separate boundaries of background labels and touching segments which is a known problem of medical image segmentation.

#### 2.2.4 Generative Adversarial Network

Goodfellow et al. (2014) proposed a deep learning framework which is called generative adversarial network (GAN) consisting of two neural networks namely generator and discriminator. The proposed network can be considered as an autoencoder trying to produce a fake version of the real data.

The generator which is the first part of the GANs, generates a sample and the discriminator interprets the sample as a real or fake. The ‘real’ means that whether the source of the data is training set. The flow can be seen in Figure 2.9.

It looks like a game where the generator tries to fool the discriminator with the samples it creates. The generator are update itself using the output of the discriminator on each iteration to get accurate results. GANs have proved its success in many image analysis tasks, such as creating very realistic synthetic images (Shrivastava et al., 2017), domain adaption (Bousmalis et al., 2017) and data completion (Yeh et al., 2017).

### 2.3 Related Works

Publication of AlexNet in 2012 have triggered a paradigm change in image segmentation, and then deep learning methods have provided prominent results and became the state-of-the-art in this area in recent years (Quang et al., 2017). In this section, the studies that propose deep architectures for skin lesion segmentation are discussed. Table 2.3 shows the summary of the discussed surveys.

Long et al. (2015) proposed an FCN from the CNNs known to be successful in semantic segmentation. They adapted well-known classification networks such as AlexNet, VGG, GoogleLeNet to fully convolutional networks. Then, to create a successful segmentation, they combined semantic details from a deep layer and the appearance details from a shallow layer to define a new skip architecture. The proposed architecture achieved remarkable results compared to state-of-the-art models on PASCAL VOC.

Ronneberger et al. (2015) built a new neural network aimed to be able to get accurate results with insufficient data by using them more effectively. U-Net, the proposed network, is based on classical FCNs and consist of two symmetric paths namely contracting and expanding which is responsible for capturing the context and enabling precise localization respectively. The new neural network proved its success with very few images by winning the International Symposium on Biomedical Imaging (ISBI) 2015 Cell Tracking Challenge. In addition to being able to work with insufficient data, U-Net offers prominent results for training duration with images with relatively higher resolutions such as 512x512. In the following years, new studies showed that the proposed U-shaped network is more successful than C-Means Clustering in ISBI 2017 challenge dataset (Lin et al., 2017).

Yuan et al. (2017) introduced an improved version of FCN model using Jaccard distance as loss function. The aim of this network is increasing segmentation accuracy with solving common dermoscopic image problems such as imbalanced skin and lesion pixels, the existence of various artifacts, and irregular lesion borders. The proposed network achieved better results than the other state-of-the-art networks in ISBI 2016 challenge and PH2 databases.

Yuan (2017) presented a new skin lesion segmentation framework base on Fully Convolutional Deconvolutional Neural Networks (CDNN). Their main focus is to improve net-

work architecture rather than pre and post processings. Rectified Linear Unit (ReLU) is used as the activation of each layer in the network except to output layer. Internal covariate shift is reduced by adding batch normalization to the output of CD layers. The proposed CDNN model won the ISBI 2017 challenge.

Yuan and Lo (2017) improved their other skin lesion segmentation architectures by using smaller kernels to optimize the discriminant capacity of their newly proposed neural network. The improved version of the previous work is evaluated on the ISBI 2017 challenge dataset and placed among the top 21 in the ranking.

Bi et al. (2017) proposed a multistage FCN to increase segmentation accuracy of classical FCNs. In this network, first stage FCN focused on learning localization information and coarse appearance, whereas second stage FCN focused on subtle characteristics of the lesion boundaries. A parallel integration method is also introduced to combine the results of the first and second stage FCNs. Yu et al. (2018) presented a novel deep neural network architecture consisting of two stages called segmentation and classification. The network combines a deep learning method with a local descriptor encoding strategy for dermoscopy image recognition. A pretrained large image dataset is used to extract deep representations of a rescaled image. After that, extracted descriptors are aggregated and encoded with a Fisher Vector to get global features. At the end, the global features are used to classify images with the help of a support vector machine. The proposed network is a fully convolutional residual network (FCRN) and took second place in the segmentation category of the ISBI 2016 challenge.

Al-Masni et al. (2018) developed a framework for skin lesion segmentation via full resolution convolutional networks (FrCN). This method eliminated subsampling layers and learned the full resolution features directly. It is tested with ISBI 2017 challenge and PH2 datasets and has achieved better results against the well-known state-of-the-art segmentation networks such as U-Net, SegNet and FCN.

Li et al. (2018) introduced a new dense deconvolutional network (DDN) for skin lesion segmentation. The proposed network is based on residual learning. It consist of three main parts namely dense convolutional layer, hierarchical supervision (HS), and chained residual pooling (CRP). Dimensions of the input and output images remain unchanged in DDLs. CRP helps to capture contextual background features while HS is responsible for improving the prediction mask. They tested the network with the ISBI 2017 dataset and it achieved 86.6% Dice coefficient indices.

Xue, Xu and Huang (2018) proposed an Adversarial Neural Network (GAN), called SeGAN, based deep neural network aimed to increase accuracy of medical image segmentation. Classical GANs are not as good as expected in providing gradient feedback to the network, because their output is single which may not represent pixel level details of images. Segmentation label maps are created with the help of newly created FCN based segmentor network with a new activation function. Another significant improvement in the proposed network is multi-scale L1 loss function aimed to extract both local and global features which represent the relations between pixels.

Peng et al. (2019) introduced a new adversarial network based segmentation architecture consisting of a CNN based discrimination and a U-Net based segmentation networks. This utilized generative adversarial network is evaluated on the ISBI 2016 challenge dataset and achieved 97.0% Accuracy rate.

Tu et al. (2019) proposed an adversarial network based deep learning framework focused on solving the imbalanced lesion-background problem. The segmentation block of the proposed network is an encoder-decoder network with Dense-Residual block. Deep supervision is utilized with a multi-scale loss function. The network is evaluated on the ISBI 2017 challenge dataset and gained better segmentation results than the other state-of-the-art methods participating in that challenge.

Tschandl et al. (2019) introduced a new FCN where pretrained ImageNet weights are being used to feed the network on ResNet34 layers which are reused as encoding layers. The evaluation results showed that using pretrained weights improved the segmentation score on the ISBI 2017 challenge dataset.

Ninh et al. (2019) proposed a SegNet architecure based FCN framework which aimed to decrease the number of upsampling and downsampling layers of classical SegNet architecture to reduce the learned parameters. The proposed network is evaluated on the ISBI 2017 challenge dataset and gained sufficient results in terms of Jaccard Index and Dice coefficient.

Mirikharaji et al. (2019) proposed a deep CNN framework focused on segmenting skin lesions. The main focus of the proposed network was the use of two different annotation set consisting of reliable and unreliable annotations. The reliable annotations are marked by experts and showed reliable segmentation results. This reweighting is done by a newly deployed meta-learning approach. The proposed network shows that using

different levels of annotation noise on weighting affects the segmentation results and model robustness positively.

Sarker et al. (2019) proposed a lightweight GAN framework, called MobileGAN, aiming to reduce the number of training parameters while keeping the segmentation accuracy high. They combined the channel attention module with the 1D non-bottleneck factorization networks for the generator part of the GAN. MobileGAN is trained with ISIC 2018 training dataset and was evaluated with ISBI 2017 challenge dataset. Compared to state-of-the-art models such as FCN, U-Net, or SegNet, the results showed that the proposed network had fewer parameters, about 2.3 million, and achieved considerable scores.

Lei et al. (2020) proposed a GAN framework aiming to increase skin lesion segmentation accuracy and won the first part of ISBI 2017 challenge. The segmentation part of the proposed GAN was construct with a skip connection and dense convolution U-Net while the discrimination part was consist of a dual discriminator module. One of the discriminators was responsible for increasing the detection of boundaries while the other one was responsible for learning the contextual informations.

Zafar et al. (2020) proposed an automated neural network architecture aimed to segment skin lesion accurately. Res-Unet, the proposed network, is a combination of two well-known neural networks in image segmentation namely U-Net and ResNet. The other major improvement in this network is using image inpainting for hair removal. It was evaluated on the ISBI 2017 challenge and PH2 datasets and gained Jaccard Index of 77.2% and 85.4% respectively.

Xie et al. (2020) introduced a CNN variant, called MB-DCNN, which consisted of three sub CNNs namely coarse segmentation network, mask guided segmentation network, and enhanced segmentation network respectively. The first network was responsible for creating coarse masks which had been used on the next network to classify the lesions. The third network was a segmentation network fedded from the second classification network. There were learning transfer between networks to increase the segmentation accuracy. MB-DCNN was tested with the ISBI 2017challenge and PH2 datasets and it achieved Jaccard index of 80.4% and 89.4%.

Table 2.2: Summary of related skin lesion segmentation surveys

Publication	Architecture	Title	Highlights
-------------	--------------	-------	------------

Long et al. (2015)	FCN	Fully convolutional networks for semantic segmentation	The first FCN implementation for semantic segmentation
Ronneberger et al. (2015)	U-Net	U-net : Convolutional networks for biomedical image segmentation	A new architecture focused on medical image segmentation
Yuan et al. (2017)	FCN	Automatic skin lesion segmentation using deep fully convolutional networks with jaccard distance	Jaccard distance bases loss function
Yuan (2017)	CDNN	Automatic skin lesion segmentation with fully convolutional-deconvolutional networks	Adding batch normalization to the output of CD layers
Yuan and Lo (2017)	CDNN	Improving dermoscopic image segmentation with enhanced convolutional-deconvolutional networks	Discriminant capacity is optimized with smaller kernels
Bi et al. (2017)	FCN	Dermoscopic image segmentation via multistage fully convolutional networks	Multistage FCN with localized responsibilities
Yu et al. (2018)	FCRN	Melanoma recognition in dermoscopy images via aggregated deep convolutional features	A pretrained dataset is used to extract deep representations of images
Al-Masni et al. (2018)	FrCN	Skin lesion segmentation in dermoscopy images via deep full resolution convolutional networks	Eliminates subsampling layers and learns the full resolution features directly

Li et al. (2018)	DDN	Dense deconvolutional network for skin lesion segmentation	Residual learning based 3 layered network
Xue, Xu and Huang (2018)	SeGAN	Adversarial learning with multi-scale loss for skin lesion segmentation	GAN based network with multi-scale loss function
Peng et al. (2019)	GAN	Segmentation of dermoscopy image using adversarial networks	Consist of A CNN based discrimination and a U-Net based segmentation networks
Tu et al. (2019)	GAN	Segmentation of Lesion in Dermoscopy Images Using Dense-Residual Network with Adversarial Learning	Dense-Residual Network based segmentation block
Tschandl et al. (2019)	FCN	Domain-specific classification-pretrained fully convolutional network encoders for skin lesion segmentation	Encoding layers are fed with pretrained weight
Ninh et al. (2019)	SegNet	Skin Lesion Segmentation Based on Modification of SegNet Neural Networks	Reduces the training parameters while keeps the accuracy
Mirikhraj et al. (2019)	CNN	Learning to segment skin lesions from noisy annotations	Reliable and unreliable annotation sets are used together
Sarker et al. (2019)	MobileGAN	MobileGAN : Skin Lesion Segmentation Using a Lightweight GAN	Reduces the training parameters while keeps the accuracy
Lei et al. (2020)	GAN	Skin Lesion Segmentation via Generative Adversarial Networks with Dual Discriminators	Dual discriminator module are used for discrimination block

Zafar et al. (2020)	Res-Unet	Skin Lesion Segmentation from Dermatoscopic Images Using Convolutional Neural Network	Combination of U-Net and ResNet
Xie et al. (2020)	MB-DCNN	A Mutual Bootstrapping Model for Automated Skin Lesion Segmentation and Classification	Consists of three sub CNNs with different responsibilities

### 3 NEURAL NETWORKS IN TUMOR DETECTION

In this section, firstly Artificial Neural Networks (ANNs), and then Convolutional Neural Networks (CNNs) are examined with the commonly used regularization techniques in the orientation of tumor detection.

#### 3.1 Artificial Neural Networks

ANNs are a category of supervised machine learning algorithms whose design has been inspired by the neurophysiological workings of the human brain (Hill et al., 1994). These networks consist of several layers mainly first layer, last layer and middle layer(s). The first layer is known as the input layer, middle layer which is called as hidden layer and the last layer is the output layer where each layer has several artificial neurons. A sample ANN model is given with two inputs, one hidden layer, and output layer with two neurons (Babu and Shailesh, 2000) in Figure 3.1. The most common layer organization is the fully connected layer, where each neuron is fully paired with adjacent neurons.

An ANN transforms the inputs into outputs using the activation function, bias and weights. The sum of inputs is multiplied by weights ; the deviation is added and the result is passed through the activation function. The neurons are activated by the activation function.

During the training, training samples are sent one by one through the network. The output value is calculated for each sample sent. Output values are compared to the tar-

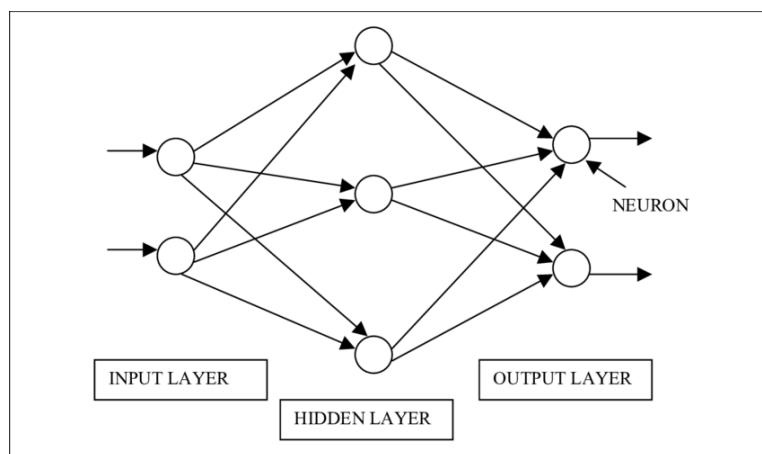


Figure 3.1: A sample ANN model

get with the help of a loss function to minimize the error rate. At the backpropagation step, the network is updated by propagating errors backwards through the network (LeCun et al., 1988).

### 3.1.1 Weight Update

Gradient descent is used to minimize the loss function of the neural network. The first-order derivative of the loss function, namely gradient is computed at the current point and it is used to increase the slope in the opposite direction by moving in by the value of self. These two steps are applied to the weights in each cycle. Batch gradient descent (BGD), stochastic gradient descent (SGD), and mini-batch gradient descent are some of the commonly used weight update methods. In SGD, the training samples are randomly shuffled, to put it another way, the weights are updated after each training sample (Bottou, 2010). On the other hand, all the training samples are used at weight update in batch gradient descent. SGD requires more calculations than batch gradient descent and it is more sensitive than the other. Because SGD is suitable for larger datasets and batch gradient descent is for the smaller datasets, mini-batch gradient descent which is a combination of SGD and batch gradient descent is developed. It uses a batch of a limited number of samples to update the weights.

### 3.1.2 Activation Functions

An activation function is used to decide whether an artificial neuron should be activated by calculating the weighted sum of its input. It decides whether the information that the neurons receive is relevant, and ignores it if not. The activation functions can be basically divided into 2 groups as linear and non-linear activation functions. Because linear functions have constant derivatives, there is no relation between the derivative of the linear function and the input value of  $x$ . Therefore, the output of functions will not be limited across any range.

The non-linear activation functions which are preferred over the linear activation functions can be seen in Figure 3.2. It helps to the model to generalize or adapt data. They are basically grouped by their curves and ranges. Commonly used activation functions such as Softmax, Sigmoid, Tanh, ReLU, Leaky ReLU and PReLU are examined in this section.

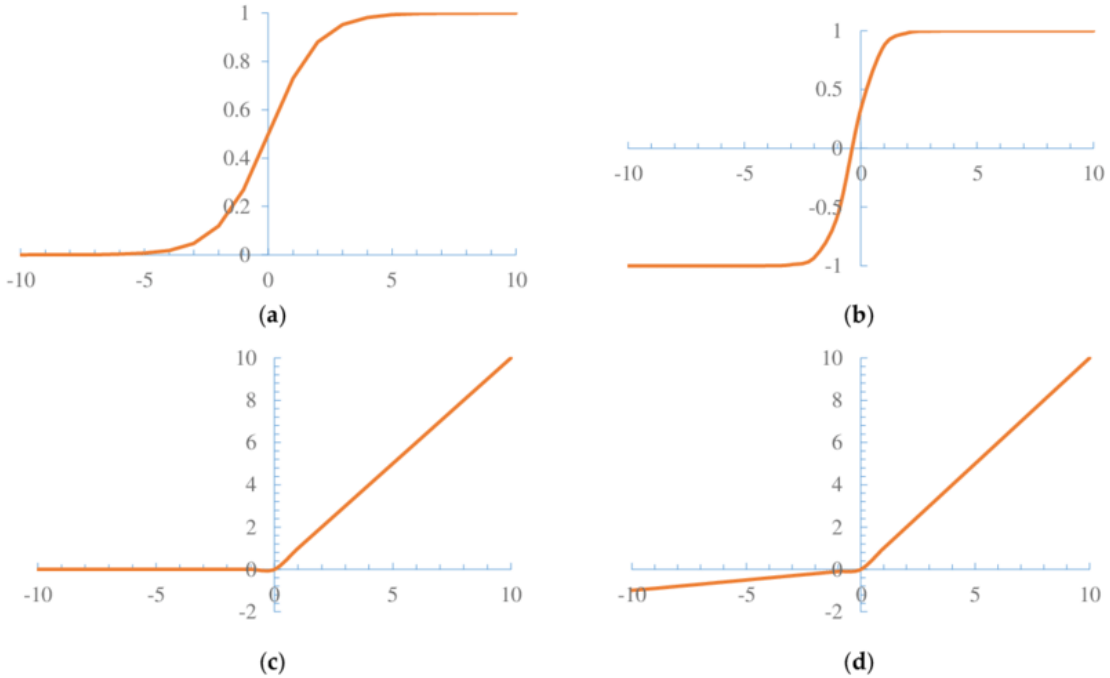


Figure 3.2: Nonlinear activation functions (a) Sigmoid, (b) Tanh, (c) ReLU, and (d) Leaky ReLU (Yang and Yang, 2018)

- **Sigmoid** functions are smooth and continuously differentiable which means the slope of the Sigmoids can be found for any two points. The Sigmoids are monotonic but their derivatives are not. In Sigmoids, the Y values tend to respond very less to changes in X as it can be seen in Equation ( 3.1). It means that small changes in the X values will cause larger changes in the Y values in this range. So the purpose of this function is to try to keep the Y values to the extremes. This is helpful when classifying the values into a particular class. If they are compared to linear functions, the outputs stay always in a fixed range [0,1] unlike the linear functions whose outputs can be in the range of infinity. It is clearly understood that the Sigmoid function produces positive values for all the points and it is not symmetric around the origin.

$$h_{\theta}(x) = \frac{1}{1 + e^{-\theta^T x}} \quad (3.1)$$

- **Softmax** is a Sigmoid function derivative which gives remarkable results in multi variant image classification.

$$y_i(z_i) = \frac{e^{z_i}}{\sum_{k=1}^K e^{z_k}} \quad (3.2)$$

- **Tanh** function is an activation function which is a scaled version of the Sigmoid function. The difference between the Sigmoid and the Tanh is that the Tanh is

symmetric over the origin whereas the Sigmoid is not symmetric, so the range of the Tanh is between -1 and 1. Continuity and differentiability of the Tanh is similar to the Sigmoid, it is continuous and differentiable.

$$\tanh(x) = \frac{2}{(1 + e^{-2x}) - 1} \quad (3.3)$$

It is preferred to Softmax if there are no more than two classes in a classification problem. The advantage is that the negative inputs will be mapped strongly negative and the zero inputs will be mapped near zero in the Tanh graph.

- **Rectified Linear Unit (ReLU)** is an activation function which is non-linear and the most widely used activation function while designing neural networks today.

$$f(x) = x^+ = \max(0, x) \quad (3.4)$$

The non-linearity makes backpropagation of the errors and have multiple layers of neurons being activated by ReLU function easy. ReLU does not activate all neurons at once. As it can be seen in Equation ( 3.4), the neuron is not activated if the input is not positive. This may cause the dead neurons problem which is the main problem of ReLU. In this activation function, only a few neurons are activated at a time. This makes the network sparse which increases the efficiency in computation.

- **Leaky ReLU** function is an improved version of the ReLU function. The gradient which is 0 for  $x < 0$  in ReLU make the neurons die for activations in that region. Leaky ReLU is focused on solving the dead neurons problem. The function is defined as a small linear component of  $x$ .

$$f(x) = \begin{cases} x & \text{if } x > 0, \\ 0.01x & \text{otherwise.} \end{cases} \quad (3.5)$$

- **PReLU** which is also known as Parameterised ReLU is very similar to the Leaky ReLU.

$$f(x) = \begin{cases} x & \text{if } x > 0, \\ ax & \text{otherwise.} \end{cases} \quad (3.6)$$

In this context,  $a$  is a trainable parameter which its values are learnt for a fast network to get an optimum convergence. PReLU is preferred when Leaky ReLU

fails to passing the relevant information to the next layer with solving the dead neurons problem.

### 3.1.3 Loss Functions

Loss function which is also called cost function evaluates the penalty between the ground truth label and the prediction during the training process to detect how well neural network models are for the dataset. The output of the loss function is inversely proportional to the success of the model, meanly higher numbers in the output are the sign of the unsuccessful model. Loss function used the error which is calculated during backpropagation to update the weights in the negative direction of its derivative.

In this section, some of the commonly used loss functions for image segmentation such as weighted cross entropy, balanced cross entropy, and Dice loss are examined.

- **Weighted Cross Entropy (WCE)** weights the classes based on the fraction of the respective class in the total dataset as it can be seen in Equation ( 3.7) which is the definition of WCE for prediction  $p$  and label  $\hat{p}$ . Thus, a class with a low fraction of the pixels in the dataset will get a high weighting. This is particularly interesting when the dataset contains unbalanced classes.

$$\text{WCE}(p, \hat{p}) = -(\beta p \log(\hat{p}) + (1 - p) \log(1 - \hat{p})) \quad (3.7)$$

$\beta > 1$  should be setted to reduce the false negative rates while  $\beta < 1$  should be setted to reduce the false positive rates.

- **Balanced Cross Entropy (BCE)** another variant of cross entropy which differs from WCE is that weighting the negative examples also.

$$\text{BCE}(p, \hat{p}) = -(\beta p \log(\hat{p}) + (1 - \beta)(1 - p) \log(1 - \hat{p})) \quad (3.8)$$

- **Dice Loss**

The values of Dice ranges from zero to one, and high value means high similarity between the segmentations. For two overlapping regions, the Dice is defined as two times the intersection over the union. Dice loss is defined in Equation ( 3.9) for prediction  $p$  and label  $\hat{p}$ .

$$DL(p, \hat{p}) = 1 - \frac{2 \sum p_{h,w} \hat{p}_{h,w}}{\sum p_{h,w} + \sum \hat{p}_{h,w}} \quad (3.9)$$

### 3.2 Convolutional Neural Networks

A convolutional neural network (also known as CNN) is a deep neural network inspired in the behavior of biological systems through artificial neurons with learnable weights and biases for image recognition tasks. D.H Hubel and T.N Wiesel discovered that the visual cortex consists of receptive fields that detect light in overlapping subregions. It is the entry point of modeling CNNs (Hubel and Wiesel, 1968). Every neuron responds to stimuli in a restricted region, as in visual cortex of the human brain, and that the overlapping regions of the neurons together cover the entire visual area.

A CNN mainly consists of different types of layers as it can be seen in Figure 3.3 including input, convolutional, non-linearity, pooling, and fully connected layers.

- **Input layer** contains input images as a matrix of the raw pixel values.
  - **Convolutional layer** is used to extract features of the input data. Each neuron has a local receptive field which means it is not fully connected, but connected to some section of the input to provide abstractions of small sections of the input data. Convolution layers calculate a dot product between the receptive field and the filter by performing convolution. The result of this convolution is a single integer which will be used as the input of the next layer.
- The filter is滑ed over the next receptive fields of the input image repeatedly until there is no unconvolved receptive field left.
- **Non-linearity layer** consists of an activation function, which applies an elementwise activation by thresholding at zero, creates and activation map with

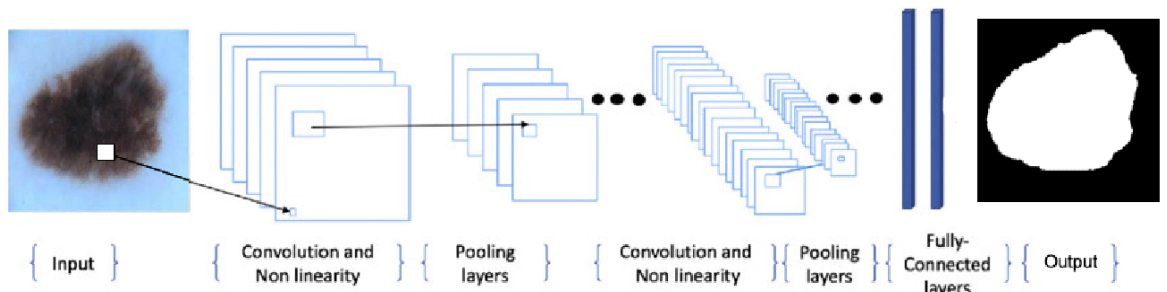


Figure 3.3: A CNN architecture for skin lesion classification

taking the output of the convolutional layer in CNNs.

- **Pooling layer** applies a spatial downsampling along the output volume. Pooling layers are commonly used to reduce the computational requirements of the neural networks progressively and minimize the overfitting.
- **Fully connected layer** mainly computes the class scores based on the training dataset. They connect the neurons in layers to each other. The last fully connected layer classifies the generated features with the help of an activation function.

### 3.3 Regularization Techniques

Commonly used neural network regularization techniques are explained in this section in details.

#### — Data Augmentation

Data augmentation is artificially boosting the diversity and number of training examples by performing random transformations to existing images to create a set of new variants without altering the meaning of the data. Flipping, rotating, adding noise are commonly used data augmentation techniques.

Data augmentation is used to prevent overfitting and especially useful when the training dataset is relatively small. While some augmentation increases the robustness of the algorithm, irrelevant transformations might make the task hard to learn, and adding new data to the training set will increase the model complexity and required time to build the model.

#### — Dropout

Overfitting is a common problem which is not limited only to deep neural networks but includes the different disciplines such as several supervised and unsupervised methods in machine learning. Neural networks can be used to create relations between their input and output to predict the newly added input with acceptable results. It can be said that there is an overfitting if the results are not good for the unknown test data but good for the training data.

Feeding the neural network with more training data is the simplest way which can be tried to prevent overfitting. This may be effective if the newly added training data bring new features which might increase the representativeness of the model. On the other hand, more training data will require more training

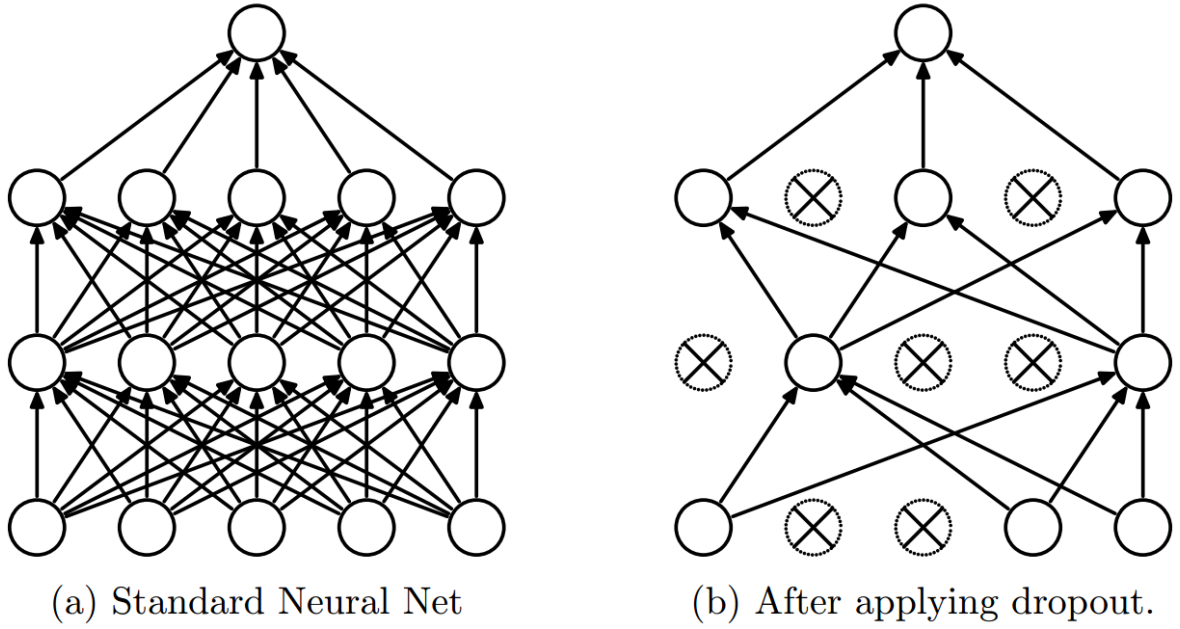


Figure 3.4: Dropout neural network model

time because it increase the model complexity. Bootstrap aggregating is another method which increase the network success (Breiman, 1996). This method classify different subsets of the training data, and fit a model based on these subsets.

Srivastava et al. (2014) said that feature vectors should be combined instead of a single feature detector in order to describe meaningful features. They found out that individual feature detectors start to detect helpful features after dropping units from the neural network randomly.

Dropout is a method of improvement which aims to increase the network performance by reducing the overfitting (Srivastava et al., 2014). At each training step, a new subset is excluded to improve the network ability for generalization. The amount of exclusion is regulated by the dropout rate. Figure 3.4 shows a regular neural network (a) and a thinned network by applying dropout (b).

#### — Weight Decay

Weight decay is another technique used to prevent overfitting by adding a regularization term such as L1 or L2 to the loss function. L1 regularization is the sum of the absolute value of the weights and produces sparse weight matrices while L2 regularization is the sum of the squares of all the feature weights and make the calculation more computationally efficient.

$$L_2 \text{ regularization term} = \|\mathbf{w}\|_2^2 = w_1^2 + w_2^2 + \dots + w_n^2$$

In L2 regularization, model complexity is dramatically affected by the outlier

weights.

#### — **Early Stopping**

Early stopping is a technique to reduce overfitting using the some part of the training data as a validation set. Training process does not include this data. If the error of the validation set reaches a certain amount, training is stopped at the training phase. It can be said that there is an overfitting exists in the current neural network for the training data.

A significant point of early stopping is the selection of validation set. It should represent all the data. It can be understood how well the model is generalizing beyond the training data.

## 4 METHODOLOGY

In this section, used dataset, neural networks, tools and frameworks are summarized and the details of the experiment are represented through the evaluation metrics.

### 4.1 Dataset

The first part of ISBI Challenge 2017 (Codella et al., 2018) - Skin Lesion Analysis Towards Melanoma Detection : Lesion Segmentation dataset is used in this thesis. This dataset has train, validation and test data separately. The training dataset consists of 2000 dermoscopic JPEG images and related masks in PNG format. The dataset includes various type of lesions such as malignant melanoma, nevus and seborrhoeic keratosis. Sample images are given with corresponding masks in Figure 4.1 where the first row represents original images and second row shows the ground truth aka the corresponding masks.

There are also validation and test datasets which contain 150 and 600 images respectively. The results are based on several common image similarity metrics which are given related section.

The images are of various dimensions and neural network model can not handle relatively big images because of the inner constraints in the architecture and memory. Therefore, all images have been resized into same dimension to reduce the memory consumption and to increase the accuracy as a preprocessing stage. As it can be stated at Figure 4.2, arrays of mask files have been converted to uint8 to reduce the size of the masks.

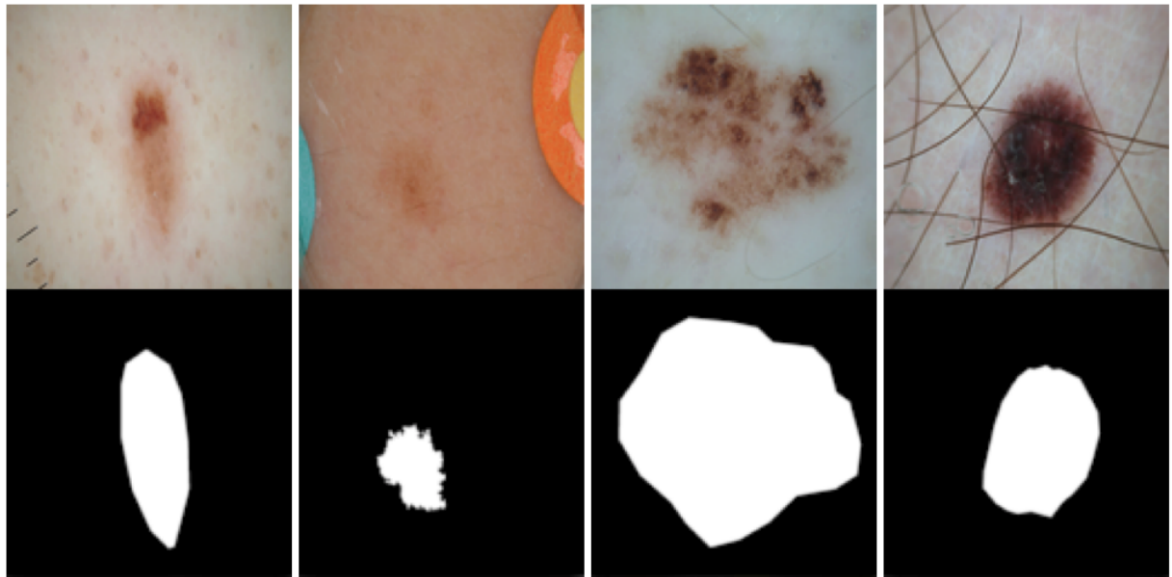


Figure 4.1: Sample skin lesions from the dataset.

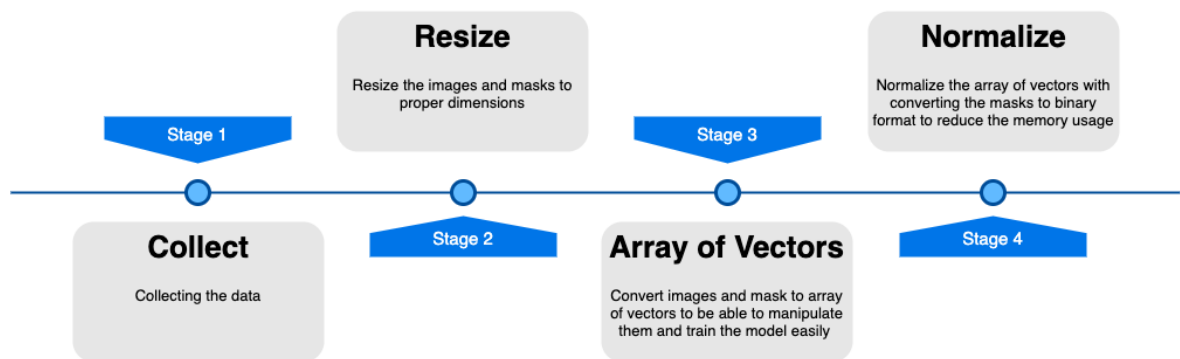


Figure 4.2: Data preparation process

## 4.2 Networks

In this section MultiResUNet and SegAN models are presented. Since U-Net architecture was considered as the baseline in this thesis, their advantages and their bottlenecks were shown through their trade-off in computation complexity and their detection performance.

### 4.2.1 MultiResUNet

As discussed in Section 2.2.3, U-Net is a state-of-the-art neural network in medical imaging, but it has some drawbacks in certain conditions. Starting from this point, Ibtehaz and Rahman (2020) proposed a new U-Net variant, MultiResUNet including several modifications examined below.

Irregularity and images in different scales are common conditions in medical imaging samples. Neural networks aiming to get accurate results in medical imaging should be able to overcome these kind of problems. Images in different scales is an ongoing situation for medical imaging even if there are some studies about it, because of that, it is not possible to say that this issue has been definitely resolved. Szegedy et al. (2015) proposed Inception architecture built on convolutional layers with various kernel size to minimize the difference of the scales between images. MultiResUNet has an improvement similar to Inception architecture. In addition to the 3x3 convolution layer in the classic U-Net, MultiResUNet has convolution layers in different kernels such as 5x5 and 7x7. Figure 4.3 shows the evolution of the MultiRes blocks with different attempts, resulting from the different uses of these kernels. These multires blocks have replaced the sequences of two convolutional layer in the vanilla U-Net.

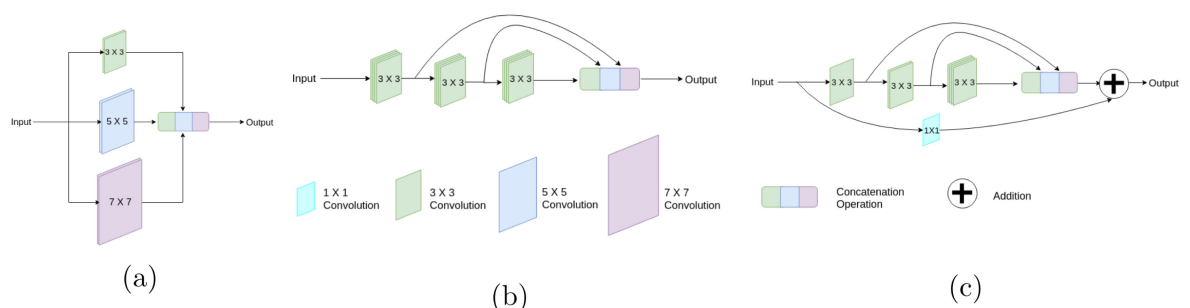


Figure 4.3: Evolution of MultiRes block : (a) Inception-like block (b) a more expensive attempt (c) MultiRes block (Ibtehaz and Rahman, 2020)

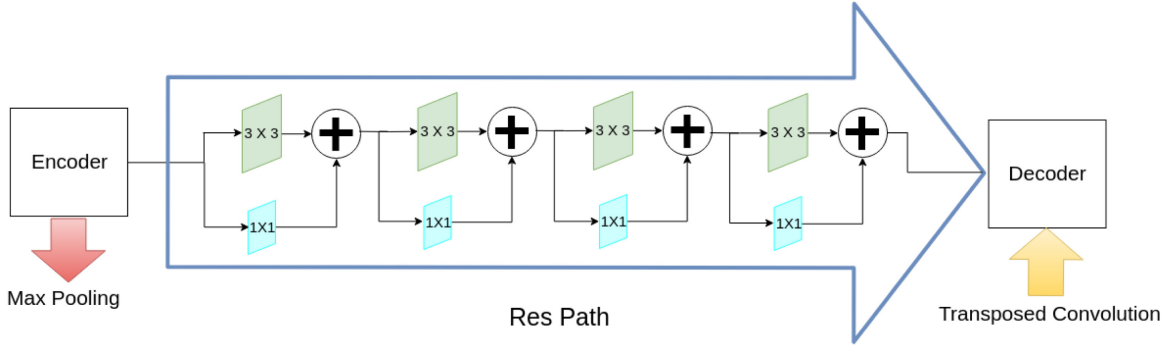


Figure 4.4: Proposed Res path with residual connections (Ibtehaz and Rahman, 2020)

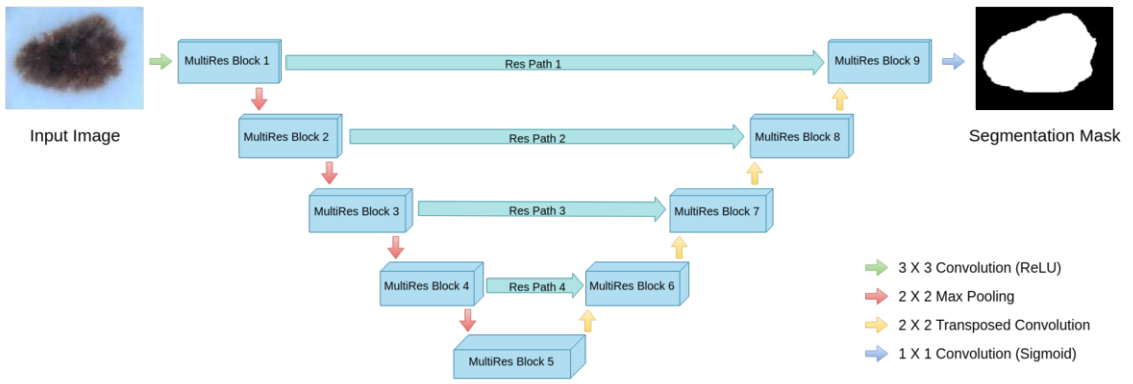


Figure 4.5: MultiResUNet architecture

One of the significant improvement in U-Net is using the skip connections between the encoder and decoder. Thus, features which are lost during pooling are recovered and transferred from encoder block to decoder block. It is expected that the features sent by encoder to decoder are low level while the features in the decoder are expected to be high level. They thought that this may cause a semantic gap between the encoder and decoder and proposed another improvement called Res path which can be seen in Figure 4.4. The proposed Res path consists of convolutional layers connected by residual connections to make learning easier (Drozdzal et al., 2016). The features are being sent from encoder to decoder are transmitted over the Res paths instead of classical skip connections of U-Net. The proposed MultiResUNet framework is shown in Figure 4.5 with the all improvements.

MultiResUNet has been tested and evaluated through several datasets including Murphy lab, ISBI 2012, ISIC 2018, CVC-ClinicDB, and BraTS17 with different modalities such as fluorescence microscopy, electron microscopy, dermoscopy, endoscopy, and MRI respectively. Their results show that the MultiResUNet offers more accurate results than the classical U-Net for the all 5 different datasets especially in dermoscopy and

endoscopy images.

#### 4.2.2 SegAN

Xue, Xu, Zhang, Long and Huang (2018) proposed a new semantic segmentation network inspired by classical generative adversarial networks (GANs). Their motivation about proposing a GAN based segmentation network is that there was no such GAN based network that give accurate results. Luc et al. (2016) have tried to segment images with a GAN-like network but explained that the network is unstable for image segmentation tasks. The creators of SegAN claim that the single scalar input, which was created by the discriminator, might the reason of the instability in image segmentation of conventional GANs. Because semantic segmentation requires pixel-level mapping, and the discriminator network of GAN may not be able to produce sufficient gradient feedback with single scalar output. The differences of the proposed network for semantic segmentation compared to classical GAN are mentioned below.

SegAN consists of two networks segmentor and critic which can be seen in Figure 4.6 similar to Generator and Discriminator networks of conventional GANs. It looks like a game as in GAN where the segmentor tries to fool the critic with the samples it creates.

The main difference arises with multi-scale loss function. While two separate loss functions are defined for generator and discriminator in GAN, segmentor and critic use a common multi-scale loss function to force the both networks of SegAN to learn local and global features which acquires relations between pixels.

The critic network aims to maximize multi-scale loss function using the differences of CNN features between the predicted images and the ground truth. On the other hand, segmentor network, which is an FCN, tries to minimize the loss function used in the critic network. They claim that the SegAN can learn spatial pixel features with the help of the proposed multi-scale loss function even the images are in different scales.

SegAN is trained with the BRATS 2015 dataset and achieved remarkable results compared to other state-of-the-art models, including U-Net, in the field of semantic segmentation.

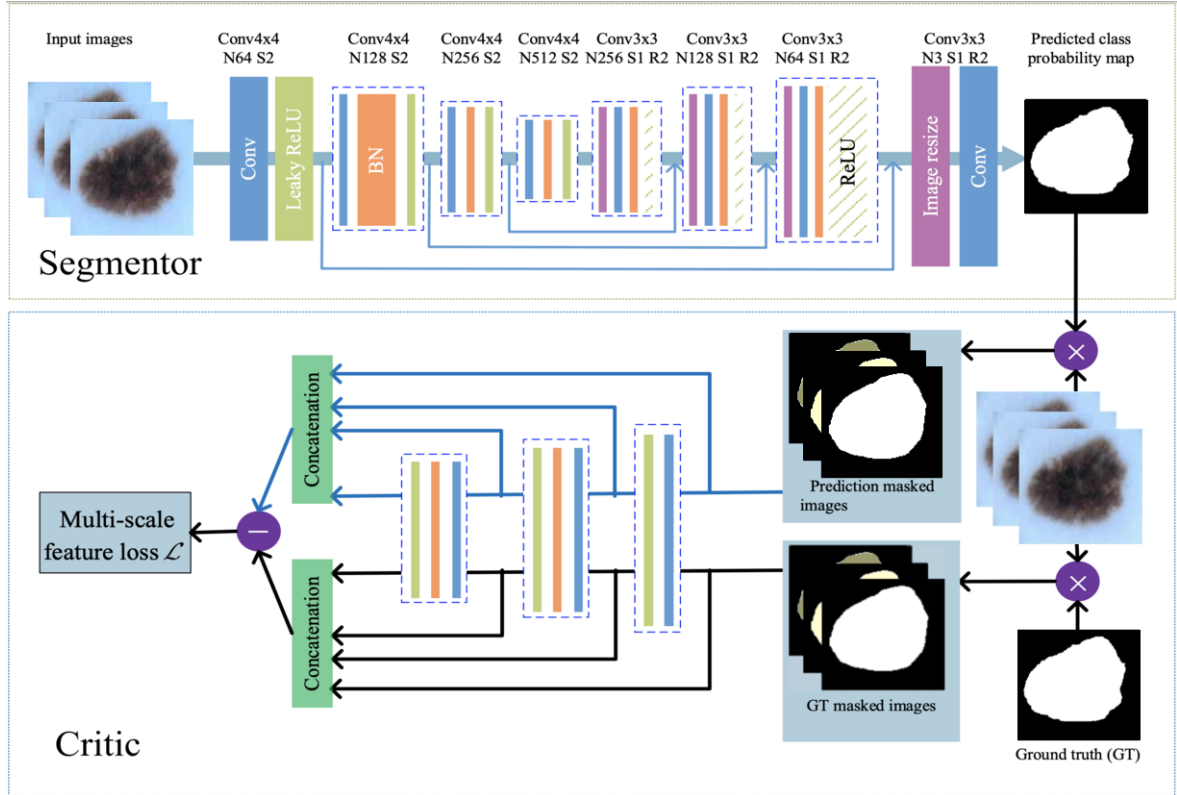


Figure 4.6: SegAN architecture

### 4.3 Tools and Frameworks

This section presents tools used for development and testing during the thesis. Python is selected as the main programming language for this thesis.

#### Tools

- **Numpy (Numerical Python)** is a scientific computing library for the Python that allows us to perform scientific calculations quickly (Oliphant, 2006). Numpy arrays form the basis of Numpy. Numpy arrays are similar to Python lists, but are more useful in terms of speed and functionality than Python lists.
- **Scipy** is a package for scientific computing which includes functionality several clustering algorithms, Fourier transforms, linear algebra, interpolation, regression, image and signal processing for the Python programming language (Virtanen et al., 2020).
- **Python Imaging Library (PIL)** is a free Python library which supports several widely-used image manipulation procedures like per-pixel manipulating, image filtering, image enhancing, masking etc (Anjal and Patil, 2019).

- **ImageMagick** is a open-source, free image editing tool that makes many morphological operation easy for more than 200 image format with its built-in features like resize, flip, transform, or special filters (*ImageMagick - Convert, Edit, or Compose Bitmap Images*, n.d.). It runs on multiple thread to increase performance and supports command-line usage that makes image editing possible for scripting languages.
- **Jupyter Notebook** is an open source web application that allows editing and running code which can be used with over 40 different programming languages (Kluyver et al., 2016). It is a Json based document that has ordered cells which can be live code, equations, visualizations or narrative text.

## Deep Learning Frameworks

- **TensorFlow** is an open source library for performing numerical computations. Although it can be used for computations in general, it is most commonly used as a tool for machine learning research. TensorFlow can be interfaced using Python and is then translated to a computational graph (Abadi et al., 2015). The computational graph can be fed with the tensors by launching a TensorFlow session which are generalization of N-dimensional arrays. Weight matrices and biases are trainable variables in the TensorFlow graph during a session. Loss functions and optimization algorithms for backpropagation exist in TensorFlow (Johansen and Pedersen, 2019). Therefore, training a model becomes as simple as specifying an objective function to optimize for, as well as running the optimizer with a batch of data inside a session.
- **Keras** is a neural networks API for Python (Chollet, n.d.). It runs on top of TensorFlow or Theano (Mohan and Subashini, 2019) which is used as the main neural network framework. Keras is user-friendly and allows for complex models to be created with relatively few lines of code. Keras consists of many commonly used building blocks of neural networks. These are parts as layers, objectives, activation functions and optimizers. The components include parts for convolutional and recurrent neural networks as convolutions, pooling, dropout and batch normalization.
- **PyTorch** is a machine learning framework introduced by Facebook which has relatively advantages over TensorFlow in terms of simplicity and usability. It implements dynamic computational graphs which makes dynamic changes on the

networks possible with a little effort. Debugging is relatively easy with Pytorch.

## Hardware Requirements

Google Colab which is also known as Colaboratory that requires no setup and runs entirely in the cloud is used in this thesis. Colab is a Jupyter Notebook environment aims to support Machine Learning and Artificial Intelligence researches for free, because this kind of process requires serious computational power. Many deep learning projects can be developed with Google Colaboratory on the default GPU processor of it, Tesla K80, using common Deep Learning frameworks and tools like Keras, TensorFlow and PyTorch. Google Colab runs on a connected Google Drive accounts. All models were trained and tested using Tesla K80 GPU which has 25 GB of video memory on a Ubuntu 18.04.

## 4.4 Experiments

Our study is composed of three steps; preprocessing, implementations of networks, and evaluation. During the preprocessing, image normalization procedures have been applied to data explained in Section 4.1; the image resizing and the conversion of file formats. Moreover, data size has been augmented by creating additional images files in different noise levels. Because our main focus is comparing the proposed network under the same conditions, the preprocessing stages were kept the same for a fair comparison of U-Net, MultiResUNet and SegAN.

Hyperparameters of training proses are explained below while the compared networks are explained in details in Section 4.2.

- **Batch size** refers to the number of samples utilized in one iteration before updating the model parameters. It looks like an iteration where the error rate is calculated at the end of the iteration by comparing the batch predictions with ground truth. The calculated error is used to update model parameters.
- **Epoch** is an hyperparameters shows the number of passes of the algorithm through the entire training data. It depends on several criteria such as problem definition and data distribution and can changed from hundreds to thousands until the error rate of the learning algorithm reduced by a certain level.

- **Learning rate** determines how much an update step affects the current value of the model weights. In other words, it is used to decide how quickly the model will forget what it has already learned.
- **Optimizers** try to minimize the loss function with the help of them by updating the model parameters.

U-Net and MultiResUnet have been trained for 200 epochs with a batch size of 8 and binary cross entropy loss function. As the performance did not increase epoch size has been kept as 200. Adam optimizer has been used as optimizer with the default parameters stated in the original paper.

Furthermore SegAN has been trained for 200 epochs with a batch size of 200 and an adaptive learning rate for Adam optimizer which started from  $2.0 \times 10^{-4}$  and multiplied by a decay rate of 0.5 every 25 epochs. Several learning and decay rates have been tried but the given parameters were found optimal like the original article.

Early stopping has been used for the all networks. If the performances of models stoped improving after a certain number of epochs, 30 was set to stop the training.

The experiments have been designed by giving additive noise into initial dataset. Five different noise levels except to noise free have been tested using Gaussian noise given as it follows through the initial image  $I_i$  ;

$$I_{final} = I_i + I_n \quad (4.1)$$

$I_{final}$  and  $I_n$  in Equation ( 4.1) are the noisy image and Gaussian noise, respectively.

The Gaussian noise is defined in the Equation ( 4.2).

$$p_G(z) = \frac{1}{\sigma\sqrt{2\pi}} e^{-\frac{(z-\mu)^2}{2\sigma^2}} \quad (4.2)$$

$p_G(z)$  denotes the noise distribution in single channel image. Our images have been encoded in RGB channels. Therefore, the noise has been applied for the all three channels.

$\mu$  and  $\sigma$  represents the mean value and the standard deviation, respectively. We used 5 noise levels for the experiments with different  $\sigma$  values from 0 to 50 by 10.

## 4.5 Evaluation Metrics

Several evaluation metrics were used to determine the quality of the models. Dice coefficient, Jaccard index, Accuracy, Sensitivity and Specificity were used to compare the target and predicted segmentation mask. The true positives (TP) determine pixels (or voxels) correctly classified as being part of the segmentation, a false positive (FP) is a pixel incorrectly classified as being part of the segmentation, and a false negative (FN) is a pixel which should have been part of the segmentation but was not.

- **Dice coefficient** which is also known as similarity coefficient or F1 score is a similarity metrics computed by comparing the pixel-wise agreement between the groundtruth and its predicted segmentation. Specially, this metric is just used to evaluate the segmentation performance of the model.

$$Dice = \frac{2 * TP}{2 * TP + FN + FP} \quad (4.3)$$

- **Jaccard index** also known as the Jaccard similarity coefficient, is a similarity metrics which compares predictions with the ground truths by dividing the size of the intersections by size of the unions.

$$Jaccard = \frac{TP}{TP + FN + FP} \quad (4.4)$$

- **Accuracy** measures the proportion of true positives and true negatives whose are correctly segmented instances to the total number of instances. It is derived from sensitivity and specificity which are given below.

$$Accuracy = \frac{TP + TN}{TP + FP + TN + FN} \quad (4.5)$$

- **Sensitivity and Specificity** are the other metrics used in this thesis. Sensitivity aims to measure correctly segmented instance ratio while specificity measures incorrectly segmented instance ratio.

$$Sensitivity = \frac{TP}{TP + FN} \quad (4.6)$$

$$Specificity = \frac{TN}{TN + FP} \quad (4.7)$$

## 5 RESULTS

Experiments show that the both SegAN and MultiResUNet achieved almost the same dice coefficient result for the noise free images but vanilla U-Net did not achieved similar results in terms of the same similarity metrics. It's not as successful as the others. MultiResUNet is slightly more successful than SegAN if they compared with Jaccard coefficient. The detailed results are given in the Table 5.1, 5.2 and 5.3 through statistical metrics. Although the dice results of MultiResUNet and SegAN are very close for the noiseless datasets, the dice results differ for the all models as the noise level increases.

Both MultiResUnet and SegAN achieved their best results around the epoch size of 50. The results were found similar after this point. Figure 5.7, 5.9 and 5.8 point out the dice results of models at different levels of epoch size. Figure 5.1, 5.2 and 5.3 show the evaluation results of dermoscopic images from the evaluation dataset with different success rates. Furthermore, Figure 5.4, 5.5 and 5.6 show the results of MultiResUNet with different success rates.

When the noise level is 50%, the dice results of MultiResUNet's decreased up to 28%, the U-Net's decreased up to 23%, while the SegAN's decreased up to 53%. As it explained in Section 4.2.1, SegAN introduces fake skin lesions during the generator level and the discriminator takes a decision after the training if test image is a lesion. The noise added during the training phase of SegAN makes the model more successful against noisy data.

Figure 5.11 shows the change of success of the models against noise. As can be seen

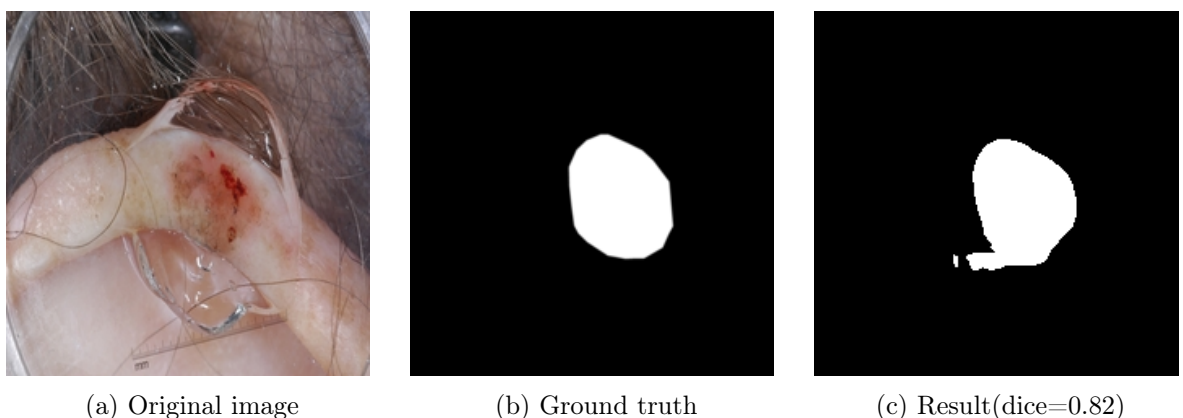


Figure 5.1: SegAN result with average score at 0% of Gaussian noise

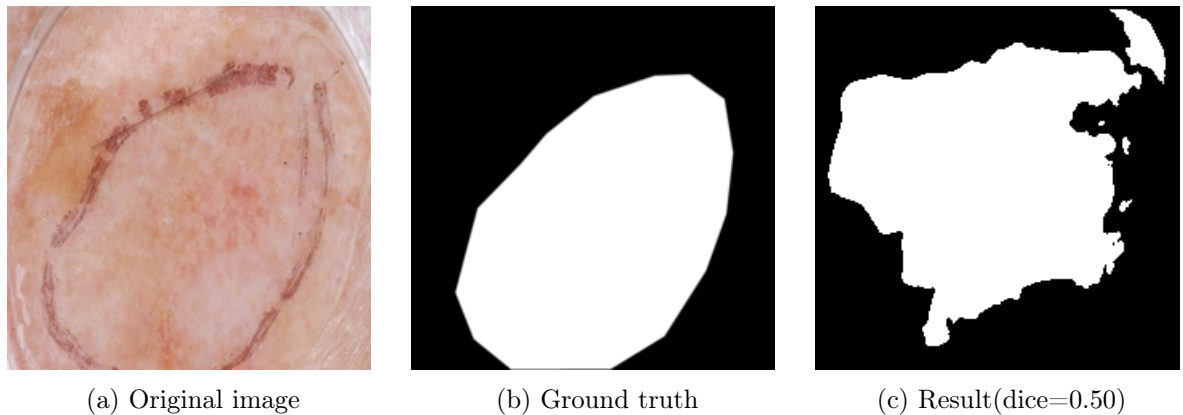


Figure 5.2: SegAN result with low success compared to average at 0% of Gaussian noise

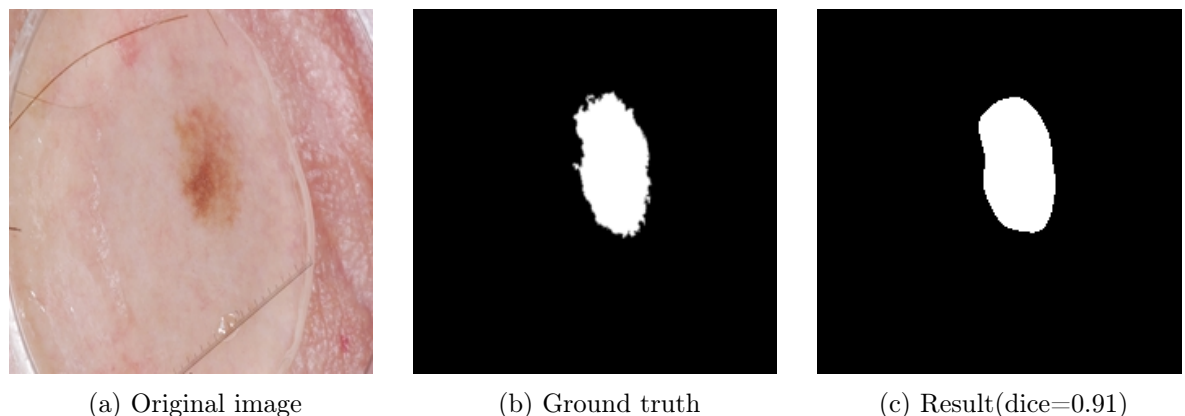


Figure 5.3: SegAN result with high success compared to average at 0% of Gaussian noise

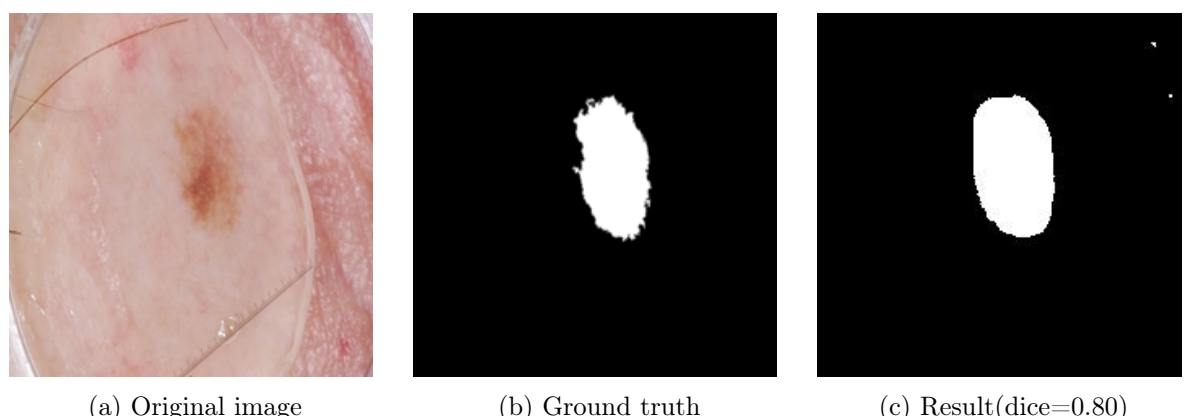


Figure 5.4: MultiResUNet result with average score at 0% of Gaussian noise

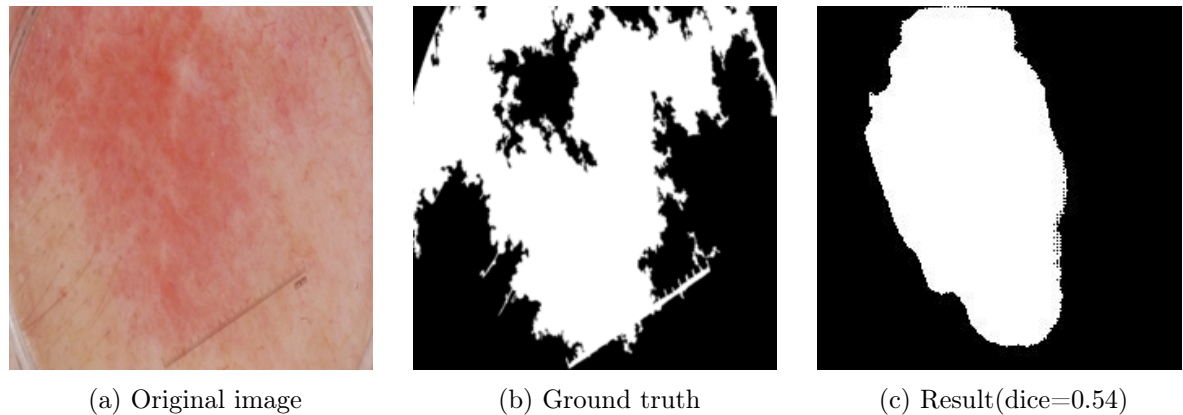


Figure 5.5: MultiResUNet result with low success compared to average at 0% of Gaussian noise

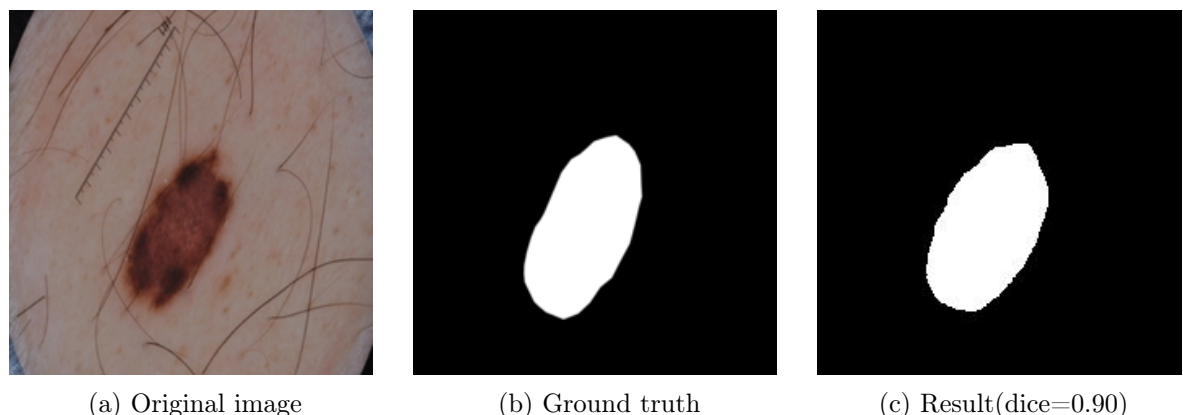


Figure 5.6: MultiResUNet result with high success compared to average at 0% of Gaussian noise

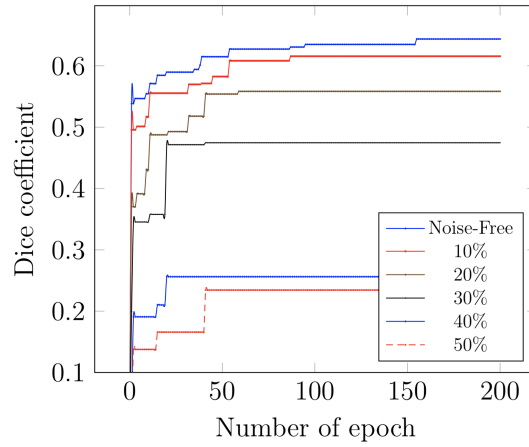


Figure 5.7: Dice results for U-Net at different Gaussian noises by number of epochs

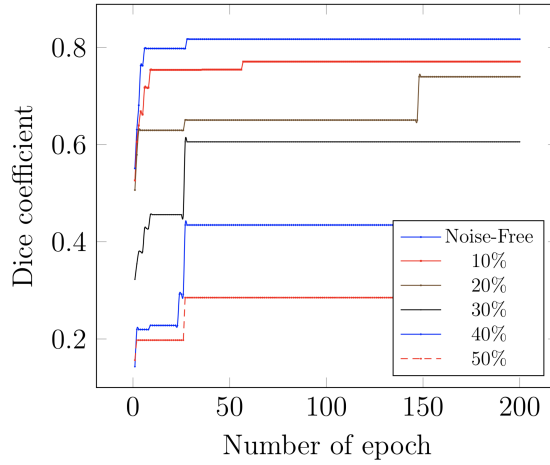


Figure 5.8: Dice results for SegAN at different Gaussian noises by number of epochs

here, SegAN is more robust than vanilla U-Net and MultiResUNet at increased levels of Gaussian noises.

Although it is not possible to create a model that fit all dataset, it is the main objective to present a model that best generalizes them Figures 5.12 and Figure 5.13 are the outputs obtained by evaluating 2 pictures with two models in different levels of noises. While SegAN give more successful results for the image in Figure 5.12, MultiResUNet is more successful in the image of Figure 5.13. As can be seen from that comparision, there is no precise superiority of the models to each other for certain data.

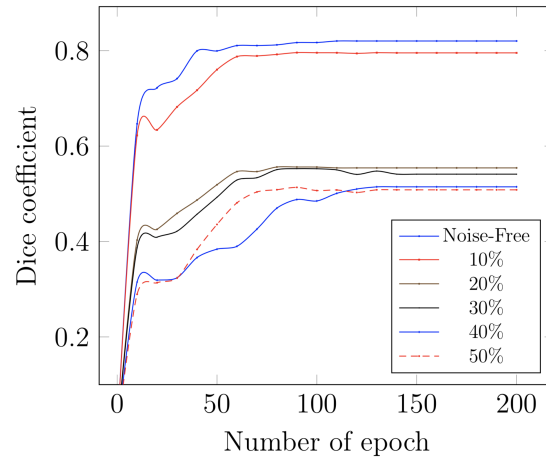


Figure 5.9: Dice results for MultiResUNet at different Gaussian noises by number of epochs

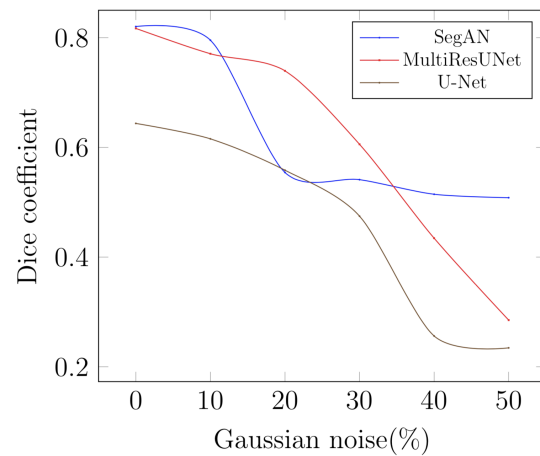


Figure 5.10: Comparision of the results of the models at different noise levels

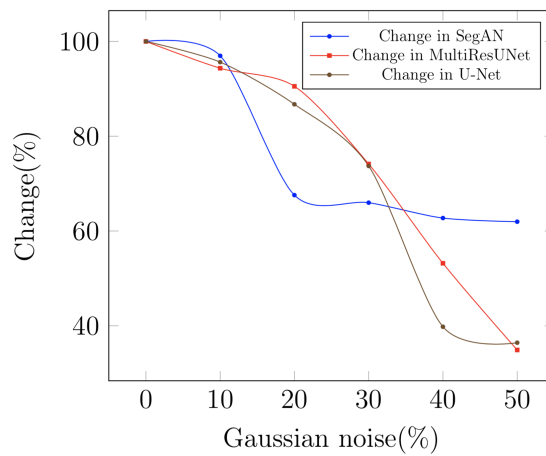


Figure 5.11: Change of success of the models by noise level

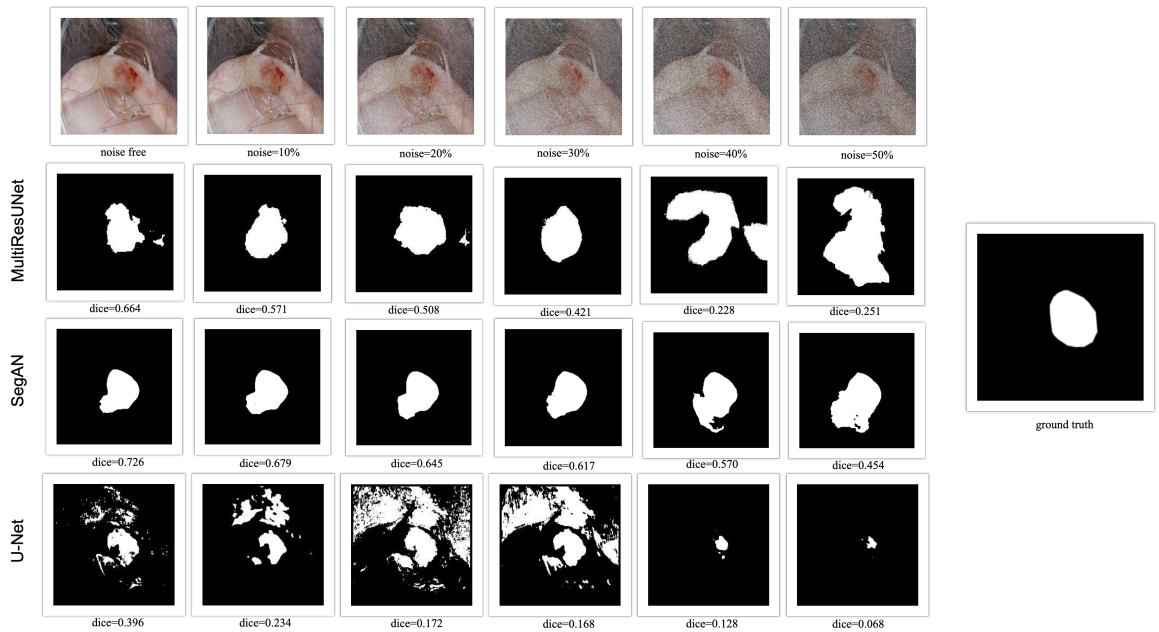


Figure 5.12: Dice results of the same image for the all networks at different Gaussian noises. The images in a column from top to bottom show the input, results of MultiResUNet, SegAN, and U-Net respectively. SegAN has better results

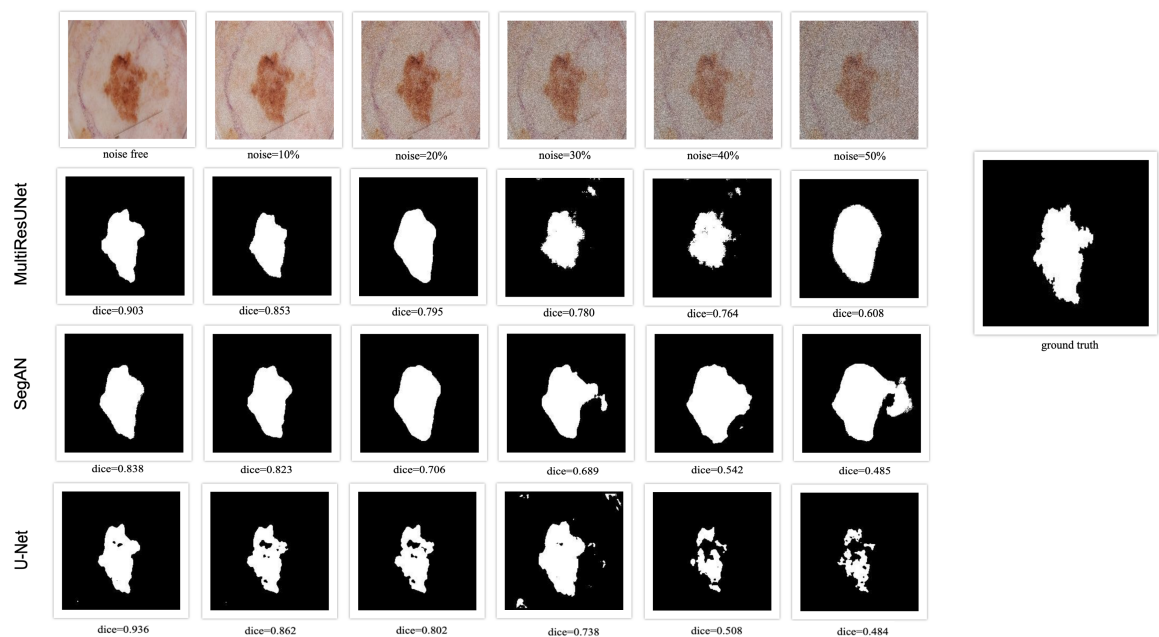


Figure 5.13: Dice results of the same image for the all networks at different Gaussian noises. The images in a column from top to bottom show the input, results of MultiResUNet, SegAN, and U-Net respectively. U-Net has better results

Table 5.1: Comparision of segmentation results of U-Net at different levels of Gaussian noise with evaluation metrics

Gaussian noise(%)	Dice	Jaccard	Accuracy	Sensitivity	Specificity
0	0.6437	0.5343	0.8619	0.7350	0.8825
10	0.6156	0.5087	0.8559	0.7562	0.8718
20	0.5584	0.4482	0.8423	0.7680	0.8507
30	0.4746	0.3707	0.8282	0.7817	0.8316
40	0.2562	0.1737	0.7853	0.6236	0.7941
50	0.2345	0.1638	0.7954	0.7575	0.7869

Table 5.2: Comparision of segmentation results of SegAN at different levels of Gaussian noise with evaluation metrics

Gaussian noise(%)	Dice	Jaccard	Accuracy	Sensitivity	Specificity
0	0.8110	0.6968	0.9236	0.8998	0.9240
10	0.5570	0.4	0.8129	0.6232	0.8445
20	0.5518	0.3936	0.8134	0.6322	0.8417
30	0.5456	0.3878	0.8132	0.6329	0.8398
40	0.5378	0.3791	0.809	0.6085	0.8442
50	0.5368	0.3783	0.8115	0.6364	0.8351

Table 5.3: Comparision of segmentation results of MultiResUNet at different levels of Gaussian noise with evaluation metrics

Gaussian noise(%)	Dice	Jaccard	Accuracy	Sensitivity	Specificity
0	0.8169	0.7221	0.922	0.964	0.9482
10	0.7707	0.6747	0.9058	0.8923	0.9024
20	0.7395	0.624	0.8829	0.8788	0.8705
30	0.6056	0.4784	0.6056	0.8402	0.7949
40	0.4345	0.3061	0.8062	0.7033	0.8104
50	0.2851	0.1969	0.7878	0.7729	0.7847

## 6 DISCUSSION

In this thesis, different neural network models have been studied by using Gaussian noise models through skin lesion dataset. The performance analysis showed the success ratio for U-Net, MultiResUNet and SegAN models.

Even if the performance of SegAN architecture was below MultiResUNet for noise free images, the segmentation through gradual noise showed that SegAN could derive better evaluation scores. The architectures used in this thesis have been observed to examine both the evaluation metrics and the reaction against the gradual noise. In the MultiResUNet architecture, the most significant improvement compared to U-Net was the multi-scale loss function. MultiResUNet and SegAN results have been compared with respect to the initial model U-Net to be able to see their behaviours. On the other hand, all models can be subjected to more detailed pre and post processing steps. It can be understood whether the models are successful only in medical images by testing all of them with different datasets. Because it is not our main purpose to extend the models success, all inner process has been set via the initial configurations of models. In this context, adding different noises to relevant points in networks such as activation functions, loss functions, weights or hidden layers can be sensible to see the results of these kind of circumstances.

Instead of choosing FCN as the segmentor network of SegAN architecture, MultiResUNet could be implemented within SegAN to extend the model and to derive an hybrid performance.

## 7 CONCLUSION

Skin lesions or tumors may have severe results in human health. The early analysis of potential moles can increase the survival rate by using appropriate detection paradigms. Advanced technologies such as deep learning are actually used in several fields in medicine to increase the diagnosis of the illnesses in the early stages. Image based analysis can help to the oncologists or the surgeons when detecting the skin tumors. It is clearly stated that the main purpose of the deep learning in medical imaging is to help to the medicians instead of replacing them. These kind of supportive methods can help to the medicians before their final diagnosis.

In this thesis, the problem of skin lesion segmentation is addressed by providing a unified hierarchy to compare several deep learning methods. Medical image segmentation has been performed using U-Net, SegAN and MultiResUNet. The dataset has created along ISIC for ISBI 2017 Challenge and has been enriched by adding Gaussian noises at different levels of sigmas. Insufficient data is a big challenge in medical imaging and this thesis aimed to provide accurate guidance, even if the dataset is insufficient. The experiment results showed that MultiResUNet and SegAN give more accurate results compared to vanilla U-Net and none of MultiResUNet or SegAN is superior to other for the all dataset.

## REFERENCES

- Abadi, M., Agarwal, A., Barham, P., Brevdo, E., Chen, Z., Citro, C., Corrado, G. S., Davis, A., Dean, J., Devin, M. et al. (2015). Tensorflow : Large-scale machine learning on heterogeneous systems.
- Al-Masni, M. A., Al-antari, M. A., Choi, M.-T., Han, S.-M. and Kim, T.-S. (2018). Skin lesion segmentation in dermoscopy images via deep full resolution convolutional networks, *Computer methods and programs in biomedicine* **162** : 221–231.
- Aljanabi, M., Jumaa, F., Aftan, A., Salah, M., Alkafaji, S., Alani, N., Al-Tameemi, Z. and Al-mamoori, D. (2019). Various types of skin tumors lesion medical imaging (stlmi) of healthy and unhealthy moles a review and computational of : Segmentation, classification, methods and algorithms various types of skin tumors lesion medical imaging (stlmi) of healthy and unhealthy moles a review and computational of : Segmentation, classification, methods and algorithms, *IOP Conference Series Materials Science and Engineering* .
- Anjal, S. and Patil, A. (2019). Roi based automated meter reading system using python.
- Babu, B. and Shailesh, M. (2000). Adaptive networks for fault diagnosis and process control, *Proc. International Symposium, 53rd Annual Session of IChE (Chemcon-2000), Calcutta*, Citeseer.
- Badrinarayanan, V., Kendall, A. and Cipolla, R. (2017). Segnet : A deep convolutional encoder-decoder architecture for image segmentation, *IEEE transactions on pattern analysis and machine intelligence* **39**(12) : 2481–2495.
- Bi, L., Kim, J., Ahn, E., Kumar, A., Fulham, M. and Feng, D. (2017). Dermoscopic image segmentation via multistage fully convolutional networks, *IEEE Transactions on Biomedical Engineering* **64**(9) : 2065–2074.
- Bottou, L. (2010). Large-scale machine learning with stochastic gradient descent, *Proceedings of COMPSTAT'2010*, Springer, pp. 177–186.
- Bousmalis, K., Silberman, N., Dohan, D., Erhan, D. and Krishnan, D. (2017). Unsuper-

- vised pixel-level domain adaptation with generative adversarial networks, *Proceedings of the IEEE conference on computer vision and pattern recognition*, pp. 3722–3731.
- Breiman, L. (1996). Bagging predictors, *Machine learning* **24**(2) : 123–140.
- Chilamkurthy, S., Ghosh, R., Tanamala, S., Biviji, M., Campeau, N. G., Venugopal, V. K., Mahajan, V., Rao, P. and Warier, P. (2018). Deep learning algorithms for detection of critical findings in head ct scans : a retrospective study, *The Lancet* **392**(10162) : 2388–2396.
- Chollet, F. (n.d.). et al. 2015. keras.
- Codella, N. C., Gutman, D., Celebi, M. E., Helba, B., Marchetti, M. A., Dusza, S. W., Kalloo, A., Liopyris, K., Mishra, N., Kittler, H. et al. (2018). Skin lesion analysis toward melanoma detection : A challenge at the 2017 international symposium on biomedical imaging (isbi), hosted by the international skin imaging collaboration (isic), *2018 IEEE 15th International Symposium on Biomedical Imaging (ISBI 2018)*, IEEE, pp. 168–172.
- Dhawan, A. P., D'Alessandro, B., Patwardhan, S. and Mullani, N. (2009). Multispectral optical imaging of skin-lesions for detection of malignant melanomas, *2009 Annual International Conference of the IEEE Engineering in Medicine and Biology Society*, IEEE, pp. 5352–5355.
- Drozdzal, M., Vorontsov, E., Chartrand, G., Kadoury, S. and Pal, C. (2016). The importance of skip connections in biomedical image segmentation, *Deep Learning and Data Labeling for Medical Applications*, Springer, pp. 179–187.
- Feit, N. E., Dusza, S. W. and Marghoob, A. A. (2004). Melanomas detected with the aid of total cutaneous photography, *British Journal of Dermatology* **150**(4) : 706–714.
- Gerger, A., Koller, S., Kern, T., Massone, C., Steiger, K., Richtig, E., Kerl, H. and Smolle, J. (2005). Diagnostic applicability of in vivo confocal laser scanning microscopy in melanocytic skin tumors, *Journal of Investigative Dermatology* **124**(3) : 493–498.
- Goodfellow, I., Pouget-Abadie, J., Mirza, M., Xu, B., Warde-Farley, D., Ozair, S., Courville, A. and Bengio, Y. (2014). Generative adversarial nets, *Advances in neural information processing systems*, pp. 2672–2680.

- Gulshan, V., Peng, L., Coram, M., Stumpe, M. C., Wu, D., Narayanaswamy, A., Venugopalan, S., Widner, K., Madams, T., Cuadros, J. et al. (2016). Development and validation of a deep learning algorithm for detection of diabetic retinopathy in retinal fundus photographs, *Jama* **316**(22) : 2402–2410.
- Guo, Y. and Ashour, A. S. (2019). Neutrosophic sets in dermoscopic medical image segmentation, *Neutrosophic Set in Medical Image Analysis*, Elsevier, pp. 229–243.
- He, K., Zhang, X., Ren, S. and Sun, J. (2016). Deep residual learning for image recognition, *Proceedings of the IEEE conference on computer vision and pattern recognition*, pp. 770–778.
- Hill, T., Marquez, L., O'Connor, M. and Remus, W. (1994). Artificial neural network models for forecasting and decision making, *International journal of forecasting* **10**(1) : 5–15.
- Hubel, D. H. and Wiesel, T. N. (1968). Receptive fields and functional architecture of monkey striate cortex, *The Journal of physiology* **195**(1) : 215–243.
- Ibtehaz, N. and Rahman, M. S. (2020). Multiresunet : Rethinking the u-net architecture for multimodal biomedical image segmentation, *Neural Networks* **121** : 74–87.
- ImageMagick - Convert, Edit, or Compose Bitmap Images* (n.d.). <https://imagemagick.org/index.php>. (Accessed on 06/06/2020).
- Işın, A., Direkoglu, C. and Şah, M. (2016). Review of mri-based brain tumor image segmentation using deep learning methods, *Procedia Computer Science* **102** : 317–324.
- Johansen, J. S. and Pedersen, M. A. (2019). *Medical image segmentation : A general u-net architecture and novel capsule network approaches*, Master's thesis, NTNU.
- Kasban, H., El-Bendary, M. and Salama, D. (2015). A comparative study of medical imaging techniques, *International Journal of Information Science and Intelligent Systems* **4**(2) : 37–58.
- Kluyver, T., Ragan-Kelley, B., Pérez, F., Granger, B. E., Bussonnier, M., Frederic, J., Kelley, K., Hamrick, J. B., Grout, J., Corlay, S. et al. (2016). Jupyter notebooks-a publishing format for reproducible computational workflows., *ELPUB*, pp. 87–90.

- Krizhevsky, A., Sutskever, I. and Hinton, G. E. (2012). Imagenet classification with deep convolutional neural networks, *Advances in neural information processing systems*, pp. 1097–1105.
- LeCun, Y., Touresky, D., Hinton, G. and Sejnowski, T. (1988). A theoretical framework for back-propagation, *Proceedings of the 1988 connectionist models summer school*, Vol. 1, CMU, Pittsburgh, Pa : Morgan Kaufmann, pp. 21–28.
- Lei, B., Xia, Z., Jiang, F., Jiang, X., Ge, Z., Xu, Y., Qin, J., Chen, S., Wang, T. and Wang, S. (2020). Skin lesion segmentation via generative adversarial networks with dual discriminators, *Medical Image Analysis* p. 101716.
- Li, H., He, X., Zhou, F., Yu, Z., Ni, D., Chen, S., Wang, T. and Lei, B. (2018). Dense deconvolutional network for skin lesion segmentation, *IEEE journal of biomedical and health informatics* **23**(2) : 527–537.
- Lin, B. S., Michael, K., Kalra, S. and Tizhoosh, H. R. (2017). Skin lesion segmentation : U-nets versus clustering, *2017 IEEE Symposium Series on Computational Intelligence (SSCI)*, IEEE, pp. 1–7.
- Long, J., Shelhamer, E. and Darrell, T. (2015). Fully convolutional networks for semantic segmentation, *Proceedings of the IEEE conference on computer vision and pattern recognition*, pp. 3431–3440.
- Lövblad, K.-O., Anzalone, N., Dörfler, A., Essig, M., Hurwitz, B., Kappos, L., Lee, S.-K. and Filippi, M. (2010). Mr imaging in multiple sclerosis : review and recommendations for current practice, *American journal of neuroradiology* **31**(6) : 983–989.
- Luc, P., Couprie, C., Chintala, S. and Verbeek, J. (2016). Semantic segmentation using adversarial networks, *arXiv preprint arXiv :1611.08408* .
- Mehmood, I., Ejaz, N., Sajjad, M. and Baik, S. W. (2013). Prioritization of brain mri volumes using medical image perception model and tumor region segmentation, *Computers in biology and medicine* **43**(10) : 1471–1483.
- Merjulah, R. and Chandra, J. (2019). Classification of myocardial ischemia in delayed contrast enhancement using machine learning, *Intelligent Data Analysis for Biomedical Applications*, Elsevier, pp. 209–235.
- Mirikharaji, Z., Yan, Y. and Hamarneh, G. (2019). Learning to segment skin lesions from noisy annotations, *Domain Adaptation and Representation Transfer and Medical Image Learning with Less Labels and Imperfect Data*, Springer, pp. 207–215.

- Mohan, G. and Subashini, M. M. (2019). Medical imaging with intelligent systems : A review, *Deep Learning and Parallel Computing Environment for Bioengineering Systems*, Elsevier, pp. 53–73.
- Ninh, Q. C., Tran, T.-T., Tran, T. T., Tran, T. A. X. and Pham, V.-T. (2019). Skin lesion segmentation based on modification of segnet neural networks, *2019 6th NA-FOSTED Conference on Information and Computer Science (NICS)*, IEEE, pp. 575–578.
- Oliphant, T. E. (2006). *A guide to NumPy*, Vol. 1, Trelgol Publishing USA.
- Peng, Y., Wang, N., Wang, Y. and Wang, M. (2019). Segmentation of dermoscopy image using adversarial networks, *Multimedia Tools and Applications* **78**(8) : 10965–10981.
- Quang, N. H. et al. (2017). Automatic skin lesion analysis towards melanoma detection, *2017 21st Asia Pacific Symposium on Intelligent and Evolutionary Systems (IES)*, IEEE, pp. 106–111.
- Ronneberger, O., Fischer, P. and Brox, T. (2015). U-net : Convolutional networks for biomedical image segmentation, *International Conference on Medical image computing and computer-assisted intervention*, Springer, pp. 234–241.
- Ruini, C., Hartmann, D., Saral, S., Krammer, S., Ruzicka, T. and von Braunmühl, T. (2016). The invisible basal cell carcinoma : how reflectance confocal microscopy improves the diagnostic accuracy of clinically unclear facial macules and papules, *Lasers in medical science* **31**(8) : 1727–1732.
- Sahuquillo, P., Tembl, J. I., Parkhutik, V., Vázquez, J. F., Sastre, I. and Lago, A. (2013). The study of deep brain structures by transcranial duplex sonography and imaging resonance correlation, *Ultrasound in medicine & biology* **39**(2) : 226–232.
- Sarker, M., Kamal, M., Rashwan, H. A., Abdel-Nasser, M., Singh, V. K., Banu, S. F., Akram, F., Chowdhury, F. U., Choudhury, K. A., Chambon, S. et al. (2019). Mobi-legan : Skin lesion segmentation using a lightweight generative adversarial network, *arXiv preprint arXiv :1907.00856* .
- Shrivastava, A., Pfister, T., Tuzel, O., Susskind, J., Wang, W. and Webb, R. (2017). Learning from simulated and unsupervised images through adversarial training, *Proceedings of the IEEE conference on computer vision and pattern recognition*, pp. 2107–2116.

- Simonyan, K. and Zisserman, A. (2014). Very deep convolutional networks for large-scale image recognition, *arXiv preprint arXiv :1409.1556* .
- Srivastava, N., Hinton, G., Krizhevsky, A., Sutskever, I. and Salakhutdinov, R. (2014). Dropout : a simple way to prevent neural networks from overfitting, *The journal of machine learning research* **15**(1) : 1929–1958.
- Szegedy, C., Liu, W., Jia, Y., Sermanet, P., Reed, S., Anguelov, D., Erhan, D., Vanhoucke, V. and Rabinovich, A. (2014). Going deeper with convolutions. corr, vol. abs/1409.4842.
- Szegedy, C., Liu, W., Jia, Y., Sermanet, P., Reed, S., Anguelov, D., Erhan, D., Vanhoucke, V. and Rabinovich, A. (2015). Going deeper with convolutions, *Proceedings of the IEEE conference on computer vision and pattern recognition*, pp. 1–9.
- Tschandl, P., Sinz, C. and Kittler, H. (2019). Domain-specific classification-pretrained fully convolutional network encoders for skin lesion segmentation, *Computers in biology and medicine* **104** : 111–116.
- Tu, W., Liu, X., Hu, W., Pan, Z., Xu, X. and Li, B. (2019). Segmentation of lesion in dermoscopy images using dense-residual network with adversarial learning, *2019 IEEE International Conference on Image Processing (ICIP)*, IEEE, pp. 1430–1434.
- Ulku, I. and Akagunduz, E. (2019). A survey on deep learning-based architectures for semantic segmentation on 2d images, *arXiv preprint arXiv :1912.10230* .
- Virtanen, P., Gommers, R., Oliphant, T. E., Haberland, M., Reddy, T., Cournapeau, D., Burovski, E., Peterson, P., Weckesser, W., Bright, J., van der Walt, S. J., Brett, M., Wilson, J., Millman, K. J., Mayorov, N., Nelson, A. R. J., Jones, E., Kern, R., Larson, E., Carey, C., Polat, I., Feng, Y., Moore, E. W., VanderPlas, J., Laxalde, D., Perktold, J., Cimrman, R., Henriksen, I., Quintero, E. A., Harris, C. R., Archibald, A. M., Ribeiro, A. H., Pedregosa, F., van Mulbregt, P. and Contributors, S. . (2020). SciPy 1.0—Fundamental Algorithms for Scientific Computing in Python, *Nature Methods* .
- Xie, Y., Zhang, J., Xia, Y. and Shen, C. (2020). A mutual bootstrapping model for automated skin lesion segmentation and classification, *IEEE Transactions on Medical Imaging* .
- Xue, Y., Xu, T. and Huang, X. (2018). Adversarial learning with multi-scale loss for

- skin lesion segmentation, *2018 IEEE 15th International Symposium on Biomedical Imaging (ISBI 2018)*, IEEE, pp. 859–863.
- Xue, Y., Xu, T., Zhang, H., Long, L. R. and Huang, X. (2018). Segan : Adversarial network with multi-scale l 1 loss for medical image segmentation, *Neuroinformatics* **16**(3-4) : 383–392.
- Yang, J. and Yang, G. (2018). Modified convolutional neural network based on dropout and the stochastic gradient descent optimizer, *Algorithms* **11**(3) : 28.
- Yeh, R. A., Chen, C., Yian Lim, T., Schwing, A. G., Hasegawa-Johnson, M. and Do, M. N. (2017). Semantic image inpainting with deep generative models, *Proceedings of the IEEE Conference on Computer Vision and Pattern Recognition*, pp. 5485–5493.
- Yu, Z., Jiang, X., Zhou, F., Qin, J., Ni, D., Chen, S., Lei, B. and Wang, T. (2018). Melanoma recognition in dermoscopy images via aggregated deep convolutional features, *IEEE Transactions on Biomedical Engineering* **66**(4) : 1006–1016.
- Yuan, Y. (2017). Automatic skin lesion segmentation with fully convolutional-deconvolutional networks, *arXiv preprint arXiv :1703.05165* .
- Yuan, Y., Chao, M. and Lo, Y.-C. (2017). Automatic skin lesion segmentation using deep fully convolutional networks with jaccard distance, *IEEE transactions on medical imaging* **36**(9) : 1876–1886.
- Yuan, Y. and Lo, Y.-C. (2017). Improving dermoscopic image segmentation with enhanced convolutional-deconvolutional networks, *IEEE journal of biomedical and health informatics* **23**(2) : 519–526.
- Zafar, K., Gilani, S. O., Waris, A., Ahmed, A., Jamil, M., Khan, M. N. and Sohail Kashif, A. (2020). Skin lesion segmentation from dermoscopic images using convolutional neural network, *Sensors* **20**(6) : 1601.

## **BIOGRAPHICAL SKETCH**

Fatih Ergin was born on August 7, 1991 in Gümüşhane, Turkey. He completed his high school education at Erzincan Anatolian Teacher High School in 2009. He obtained his bachelor degree in Computer Engineering with his study on "Collaborative Filtering Based Recommendation Systems" from Istanbul Technical University, Turkey in 2014.

## **PUBLICATIONS**

Ergin, F., Parlak, B. (2020). A Deep Learning Model for Skin Lesion Analysis using Generative Adversarial Networks, *INFUS 2020*